Procurement Executive - Ministry of Defence

AWRE, Aldermaston

AWRE REPORT No. 054/78

On the Use of Seismometer Arrays to Locate Sources of Higher Mode Rayleigh Waves

B J Barley

ISBN 0 85518128 1

CONTENTS

SUMMARY

This report is an empirical study of higher mode Rayleigh wave (R_i) data, recorded at two arrays of short period, vertical component seismometers. Our aim has been to deduce some "average" properties of R_i, such as coherence, phase velocity and relation between arrival azimuth and known back bearing to source. These properties are relevant to any future design of arrays intended to locate sources of R_i waves, observed at regional distances of 1000 to 2000 km. To this end, we cross-correlated individual traces with the remaining partial array sum, to determine the peak correlation time and the associated correlation coefficient. A least squares estimate of the R_i arrival azimuth was formed from the times at each pit, assuming a common arrival azimuth for all signal components but allowing phase velocities to vary. While the resulting arrival azimuth has small variance ($<< 1°$), the known back bearing to source often differs from this estimate by 5° or more. Average values of the correlation coefficient at each pit were plotted against pit separation. High average correlation coefficients of 0.8 or more were obtained for a substantial number of R_i arrivals per event for array apertures of 20 km or less. Taken together with the regional properties of S (a source of interference), and the range of R_i phase velocities encountered (3.5 to 5.0 km/s), these properties suggest the adoption of 10 km aperture arrays with a 1 km inter-seismometer spacing, situated at 10° to 20° epicentral distance from source regions of interest.

1. INTRODUCTION

Since the early 1960's most of the UK work on methods of discriminating between earthquakes and underground explosions by seismological means has concentrated on finding methods that can be applied to data recorded at teleseismic distances - say, epicentral distances (Δ) of greater than 30°. Recently, there has been a resurgence of interest in using seismological data recorded at regional distances, say, up to $\Delta = 20°$. Whether discrimination between earthquakes and underground explosions can be done successfully at regional distances has yet to be demonstrated. At present the main advantage of using regional data seems to be that it allows much weaker seismic sources to be detected and located than is possible using teleseismic data only. This study is concerned with source location at $10° \leq \Delta \leq 20°$ using short period (SP) array observations of higher mode Rayleigh waves.

Short period Rayleigh waves are rarely detected teleseismically, but are often the most prominent feature of vertical component SP seismograms at closer range. As the phase with the largest signal-to-noise ratio (S/N), these Rayleigh waves are potentially useful for detecting and locating weak seismic sources. As an illustration of this, figure 1 shows three component sets of seismograms for two earthquakes almost coincident in space and time; the P wave from the second is lost in the coda of the first, but the arrival of higher mode Rayleigh waves is clearly apparent.

Panza and Calcagnile [1] refer to the ith mode, j^{th} group velocity minimum of higher mode Rayleigh waves as $L_g(i,j)$. We prefer to call such arrivals R_i, and to reserve the name L_g for Love waves, as was originally intended [2]. Appendix A summarises the evidence that observed R_i and L_g phases represent different wave types despite their similar group velocities. For the purpose of this study, it is enough to note that L_g can appear only rarely on vertical component seismograms (eg, when a dipping interface is present on the path), and that the vertical component disturbance having group velocities U = 3.6 to 3.1 km/s is primarily due to arrivals of R_i type.

The data used in this report come from the short period arrays at Yellowknife, Canada (YKA) and Gauribidanur, India (GBA). These are medium aperture (∿ 20 km) arrays designed to study teleseismic P waves. Intuitively, one would expect these arrays to be less than optimal for R_i studies (because R_i has very different properties from teleseismic P), and this expectation is confirmed in practice. A major theme of this study is accordingly the analysis of R_i data from existing arrays, seeking to quantify those "average" signal properties which will constrain any future design of arrays intended to study mainly R_i waves.

The need for an empirical study of R_i arises because, like all seismic signals, R_i is "imperfectly coherent" across a real array. By this we mean that the peak value of the normalised cross-correlation function for signals recorded at two different sites in an array is never unity, but neither is its average value as low as that expected for random noise; there is no purely deterministic or purely statistical model which can adequately describe the relevant signal properties. Therefore, rather than making a theoretical analysis or numerical simulation of the array response to ideal signals (as did, for example, Birtill and Whiteway [3] who assumed perfect coherence), we study the response of established arrays to real signals.

The qualitative effects of imperfect signal coherence are easily understood. As we increase an array's dimensions beyond some arbitrarily defined coherence length at a given signal frequency, a point is eventually reached where it is no longer possible to obtain useful estimates of the velocity of the signal because the relative arrival times of the signal measured by correlation methods have errors with such a large variance that the uncertainties in the velocity estimates are also large. Conversely, as we decrease the array aperture below the coherence length, the correlation between all seismometer signal pairs increases so that the errors in the relative arrival times decrease but uncertainty increases because the time for the signal to cross the array is small. Somewhere between these two extremes of the ratio between array aperture and coherence length lies an optimum for a particular site, wavetype and form of array processing, which it is the main aim of array design to achieve.

2. DATA

The layout and scale of the YKA and GBA arrays is shown in figure 2, and their equipment is described by Mowat and Burch [4]. It

may be important that these arrays are sited on simple shields, that is, parts of the crust which have lain undeformed for more than 200 million years. The local geology is characterised by flat-lying and internally homogeneous crustal layering, without a cover of drift or variable thicknesses of recent sediments. P signals observed at the simple sites at YKA and GBA seem to be more coherent over 25 km (the aperture of these arrays) than the P signals observed at sites with more complex geology, such as the Large Aperture Seismic Array (LASA) in Montana, USA and the Norwegian Seismic Array (NORSAR) in Norway. (The LASA site lies on the eastern flanks of the Rocky Mountains, an area of recent large-scale movements, and the NORSAR array in its original form spanned the major structural feature, the Oslo Graben). It thus seems likely that the higher coherence of the P signals at YKA and GBA compared to those observed at LASA and NORSAR is a consequence of the relatively simple geology at YKA and GBA. If this is true, then in extrapolating from the results given below on R_i coherence it should be remembered that the results may only apply to arrays at sites similar to YKA and GBA.

Useful explosion data are available only for explosions at the Nevada Test Site (NTS), observed at YKA ($\Delta = 25°$), but earthquake data are plentiful at $10° < \Delta < 20°$ at both YKA and GBA. Thirty second time windows of the R_i wavetrain, starting at $U = 3.5$ km/s, were digitised at 20 samples/second and used as input to a computer program provided by Mereu and Ram [5]. The program adaptively processes array data to estimate the arrival azimuth (AZZ) and slowness (SL) of imperfectly coherent signals. The processing is iterative and, for stability, requires initial estimates of AZZ and SL which are close to the true values [6]. The events used here have known epicentres, so that the known great circle azimuth provides a good starting value for AZZ, but AZZ would have to be estimated from the data if the array was used operationally for source location. A suitable technique to provide an initial estimate of AZZ is described by Birtill and Whiteway [3], involving the cross-correlation of two partial array sums for a search pattern of phase delays and monitoring the peak value. The reason that we use adaptive processing in series with the Birtill and Whiteway technique is that, in practice, the former has a higher resolution [6]. (The transverse error in epicentre location is proportional to the error in AZZ multiplied by the radial distance from the array.) In addition, the adaptive processing program written by Mereu and Ram [5] can, with trivial modifications, be used to study R_i coherence as well as SL and AZZ.

3. DESIGN OF THE EXPERIMENT

The design of our experiment to measure R_i coherence is affected by the observed properties of S and R_i waves, the layout of the arrays used, and the choice of an adaptive form of processing. Where necessary, this section anticipates results in order to clarify the restrictions imposed.

3.1 Epicentral distances studied

The coda of S is slow to decay, and S type arrivals often contaminate the R_i wavetrain at short range (eg, at $\Delta = 8°$ in figure 1). The variable efficiency of S_n propagation across shields as compared to tectonic regions [7] will cause the precise value of Δ at which

contamination is serious to depend on the path. In general, the R_i onset (typical group velocity U = 3.6 km/s) becomes distinguishable from the S coda at $\Delta \approx 10°$. The frequency response of the SP seismometers used here is given in figure 3. In the resulting seismograms, S and R_i at $\Delta \approx 10°$ have typical dominant frequencies of 2 to 5 Hz and 1 to 2 Hz or less respectively. By band-pass filtering, this tendency towards frequency separation of S and R_i can be exploited to partially suppress S energy in the R_i wavetrain. The band-pass used to process R_i in which the S coda is discernible is 2.0 to 0.3 Hz, otherwise 3.0 to 0.3 Hz. The lower frequency limit excludes longer period microseisms.

An upper limit on the Δ of interest arises from the relative rates of decay of the P and R_i amplitudes with Δ. At large Δ, such that the P amplitude and hence S/N is greater than for R_i, P is the more useful phase for purposes of detection and location. For shallow focus events and for the paths encountered here, R_i seems to have smaller SP amplitudes than P at $\Delta \gtrsim 20°$. We shall nonetheless present results at $\Delta = 25°$ for R_i from the NTS at YKA, because R_i array data for nuclear explosions are scarce, and any results are of interest.

3.2 The existing seismometer spacing

The mean seismometer separation at YKA and GBA is about 2.3 km. This spacing determines the R_i wave numbers at which spatial aliasing can occur, when correlation methods in a narrow frequency band can produce spurious results. Consider two extreme, but not implausible, cases (the phase velocities quoted are anticipated results):-

(a) R_i with dominant frequency f = 2.0 Hz and phase velocity c = 3.5 km/s.

(b) R_i with f = 0.5 Hz, c = 5.0 km/s.

The minimum spacing x to prevent spatial aliasing in case (a) is $\frac{1}{2}x_a = f/c$, so $x_a \approx 0.9$ km and, for case (b), $x_b = 5.0$ km. Therefore, values of AZZ and SL deduced by correlation methods for case (a) R_i waves at YKA and GBA (x = 2.3 km) may be unreliable. (YKA and GBA were designed to study the longer apparent wavelengths of teleseismic P.) In the more typical case of R_i with $f \approx 1$ Hz and $c \approx 4.5$ km/s, x = 2.3 km, and YKA and GBA have adequate seismometer spacings. As is discussed in the following two sections, it is generally possible to prevent or at least detect aliasing if the signal has a wide enough bandwidth.

3.3 Problems peculiar to correlation methods of array processing

Adaptive processing [6] consists of an iterative least squares fit of a plane wavefront to the signal arrival times at each seismometer. These arrival times are determined by cross-correlating each seismometer output in turn (in a limited range of shifts) with the remaining partial array sum, and adding back the single channel at the shift where peak correlation occurs. The process is repeated until the change in the arrival times becomes small enough to neglect. The starting values of AZZ and SL must be quite close to those of the signal processed. If they are not, the program picks out the peak correlation accessible in its limited

search window, missing the significant correlation peak at the true signal phase velocity, and is misled in its subsequent refinement of the beam. A spurious correlation is pursued if the initial error of alignment in forming a beam is greater than the half period of the correlation function, and the significant correlation peak falls outside its search window. In theory, the problem can be circumvented by providing a large enough search window.

Consider an R_i wavetrain crossing an array aperture D km with a range of mode slownesses $0.3 < SL < 0.2$ s/km and processed using a starting value of SL = 0.25 s/km (SL = 0.3 s/km is equivalent to $c \approx 3.5$ km/s, and SL = 0.2 s/km is equivalent to $c \approx 5$ km/s), then the range of possible misalignments is ± 0.05D s, necessitating a search window $\tau > 0.1D$ s long if the correlation peak for all slownesses is to be defined by lower values to either side. $\tau = 0.11D$ s will serve as a rule of thumb for R_i waves processed by this method. As pointed out above, the provision of an adequate τ theoretically prevents aliasing due to initial errors in the phase delays. This statement assumes that a distinct maximum of the cross-correlation function occurs at phase delays corresponding to the signal phase velocity. If, however, the signal spans only a narrow bandwidth (so that the cross-correlation is effectively that of sinusoids), several comparable peaks of the correlation function may occur inside the search window, and aliasing is possible. Since the SP response drops rapidly below 1 Hz (figure 3), while R_i at $\Delta > 10°$ commonly have dominant frequencies less than 1 Hz, there is a tendency for the resulting SP seismograms to be narrow band. Thus, in practice, aliasing can sometimes occur. Seismometers with a broader response than the SP are therefore desirable in R_i studies. Aliasing for a wide band signal can usually be detected by the low peak correlation coefficient which results, as is now discussed.

4. MEASUREMENT OF R_i COHERENCE

We define a cross-correlation function

$$\phi_{ij}(\tau) = \int_t^{t+T} s_i(t)s_j(t+\tau)dt$$

for the time series $s_i(t)$ and $s_j(t+\tau)$. In normalised form, $\phi_{ij}(\tau)$ gives $C_{ij}(\tau)$, the cross-correlation coefficient

$$C_{ij}(\tau) = \frac{\phi_{ij}(\tau)}{\overline{s_i^2(t)}\ \overline{s_j^2(t)}}.$$

Here $\overline{s_k^2(t)}$ is the mean square of $s_k(t)$. We refer to the peak value of $C_{ij}(\tau)$ as C_{ij}. Now the adaptive processing program cross-correlates a 2 s time window from the ith channel ($s_i(t)$) with a 2 s window from the depleted sum ($s_j(t)$), that is, the total array sum minus channel i. The 2 s time windows are chosen to follow a given arrival across the array, isolating it at its particular phase velocity. This "locking-on" property of adaptive processing is extremely useful because the R_i wavetrain represents a mixture of modes, each with its own phase velocity (figure 4).

For each 2 s time window all possible values of C_{ij} are computed. If the average of these values is greater than 0.8, the time window is assumed to contain a significant arrival and so SL and AZZ are computed. Average values of $C_{ij} < 0.8$ are thought to be untrustworthy. (Cleary et al. [8] rejected measurements of AZZ and SL for which the average of C_{ij} over the array is less than 0.8. This threshold of acceptance appears to have been chosen programatically, being sufficiently high to exclude aliased signals or noise, but low enough to admit most of the imperfectly coherent signals admitted by the main lobe of the array response.) An alternative approach would be to weight the equation of condition so that less reliable observations are given less weight. The most desirable form of weighting would be to divide each equation of condition by the reciprocal standard deviation of the corresponding arrival time of R_i. However, the near impossibility of estimating the latter quantity in this experiment prevented us from using this approach. The imposition of a threshold of average C_{ij} at which data become acceptable is equivalent to using a unit step weighting function, $W_{ij} = 1$, if the average C_{ij} is greater than 0.8, and zero otherwise. If we use time windows much larger than 2 s, several arrivals with different phase velocities may be included in the correlation window, so C_{ij} will be less than unity not only because a coherent mode is not perfectly coherent, but also because of differences between channels due to mode velocity dispersion.

The adaptive processing program thus picks out significant individual arrivals and computes their slowness and azimuth and gives values of C_{ij} which contain information about signal coherence. As the depleted sum $(s_j(t))$ is only weakly dependent upon which single channel is chosen as $s_i(t)$, $s_j(t)$ can be taken to be a more or less fixed reference against which each $s_i(t)$ is correlated. We assume that the reference signal represents the signal at the centre of gravity (CG) of the array.

To measure the fall off of coherence with increasing array size we use the computed values of C_{ij} as follows. Consider channel i; all the values of C_{ij} for this channel for the arrivals in a given signal are averaged to give a measure of the coherence of channel i; we denote this quantity by $\bar{C}_{ij}$. This method of measuring signal coherence has been applied to the R_i seismograms from six earthquakes and two explosions: four earthquakes and two explosions were recorded at YKA, and the other two earthquakes at GBA. The SL and AZZ estimates obtained from the adaptive processing of these R_i seismograms are given in figures 6, 8, 10, 12, 14, 16, 18 and 20. The measures of signal coherence $\bar{C}_{ij}$ for each seismometer channel are plotted separately for each R_i seismogram against the distance of the seismometer from the CG of the array; these plots are shown in figures 7, 9, 11, 13, 15, 17 and 19 and the values of $\bar{C}_{ij}$ are listed in tables 1 to 8.

The confidence limits shown on $\bar{C}_{ij}$ could not be derived in the usual way, because the correlations are bounded by unity, and so are not normally distributed. However, a variable Z defined from the correlation r as

$$Z = \tfrac{1}{2}[\ln (1 + r) - \ln (1 - r)]$$

is distributed almost normally, and is practically independent of the value of the correlation in the population from which it is drawn.

Confidence limits for the correlations were found by computing upper and lower bounds one standard deviation away from the mean in Z and converting back to correlation r by the transformation r = tanh (Z).

A best estimate of the back bearing from the array to the epicentre is given for each event, assuming that the R_i waves travel along the great circle path, so that our best estimate of arrival azimuth is also that of the source back bearing. The way in which we arrive at these estimates is described in appendix B. For interest, an estimate of epicentral distance based on the P - R_i time is also given, assuming a group velocity for R_i onset of 3.6 km/s together with the JB times for P (figure 5). Onsets were picked by eye from the array sum. The resulting epicentral location is compared with the known locations, and the results are discussed in the final section.

5. DISCUSSION

Earlier sections have discussed the array spacing required to prevent spatial aliasing during adaptive processing of R_i (about 1.0 km), and the interference of S at shorter ranges ($\Delta \lesssim 10°$). The latter interference suggests the adoption of "stand-off" arrays purposely sited at least 10° from possible sources of R_i waves. This minimum separation has the advantage that (in many parts of the world) receivers can be sited on shield-like crust while monitoring earthquake regions, and makes a sparse network of arrays into an optimal as well as an economical proposition.

GBA has an effective aperture $1\frac{1}{2}$ times that of YKA. By this, we mean that the maximum separation of a pair of seismometers is 33 km at GBA (R10-B10), but only 22 km at YKA (R1-B10). Referring to figure 2, we see that this is because the crossover point of the array arms at YKA is at R8/B5, while it is at B1/R1 at GBA (both arrays have the same length of arm). An average of only about five solutions per 30 s of R_i wavetrain were obtainable at GBA using all seismometers (remember that only those signals showing $C_{ij} > 0.8$ are accepted), but when R8-R10, B8-B10 were ignored, this average rose to be comparable with YKA. The results given for GBA apply to this reduced aperture. This is a pleasing result, because it seems to confirm the general downward trend in $\bar{C}_{ij}$ with increasing distance apparent in figures 7, 9, 11, 13, 15, 17, 19 and 21.

The downward trend in $\bar{C}_{ij}$ is most apparent for the higher frequency R_i, as expected; the low frequency R_i from NTS at YKA does not show this trend. The critical array aperture thus appears to be about 20 km. It is pointless to increase the aperture further, because correlation methods cannot then be trusted to relate distal and proximal signals to the arrival azimuth of R_i. (This statement applies to the high frequency ($\sim$ 1 Hz) R_i; for the low frequency (0.5 Hz) R_i from NTS explosions at $\Delta = 25.3°$, YKA has a smaller than critical aperture. However, usually the predominant frequency of R_i is around 1 Hz at $10° < \Delta < 20°$, and this is the type of data on which we design an array.)

Now the numerical precision with which a 22 km aperture array can estimate R_i arrival azimuths has been shown to be generally much less than the difference between the great circle azimuth and the experimentally determined estimate of the arrival azimuth. The latter difference is probably due to lateral refraction, akin to that commonly observed for

LP fundamental mode Rayleigh waves. These path effects introduce an uncertainty in source location which no amount of instrumentation at one site can reduce. This is to say that the array aperture (and hence velocity and azimuth resolution) could have been decreased without loss of accuracy in source location. Again, this reduction in array aperture is desirable because the smaller the array, the lower the cost.

A 20-seismometer array of 10 km aperture with inter-seismometer spacing of about 1.0 km would thus seem to be about optimum for studying R_i.

This is the specification of the SP array at Eskdalemuir (EKA) in Scotland, which was designed to study P waves in the first zone. It therefore appears that an array similar to EKA can optimally combine the study of both P and R_i waves in the first zone.

6. ACKNOWLEDGMENTS

Acknowledgments are due to Mr A Douglas for his derivation of the least squares theory of appendix B, and to Messrs R G Pearce and P D Marshall for help with data preparation.

REFERENCES

1. G F Panza and G Calcagnile: "Lg , Li and Rg from Rayleigh Modes". Geophys J R Astr Soc, 40, 475-487 (1975)

2. F Press and M Ewing: "Two Slow Surface Waves across North America". Bull Seis Soc Am, 42, 219-228 (1952)

3. J W Birtill and F E Whiteway: "The Application of Phased Arrays to the Analysis of Seismic Body Waves". Phil Trans Roy Soc, 258, 421-493 (1965)

4. W M H Mowat and R E Burch: AWRE Report 44/47/29 (1974)

5. R F Mereu and P Ram: "A Computer Program Package for the Analysis of Array Data Using Adaptive Processing Techniques" in "Expoitation of Seismograph Networks". NATO Advanced Study Institutes Series E, No. 11 (1975)

6. D W King , R F Mereu and K Muirhead: "The Measurement of Apparent Velocity and Azimuth using Adaptive Processing Techniques on Data from the Warramunga Seismic Array". Geophys J R Astr Soc, 35, 137-167 (1973)

7. P Molnar and J Oliver: "Lateral Variations in Attenuation in the Upper Mantle and Discontinuities in the Lithosphere". J Geophys Res, 74, 2648-2682 (1969)

8. J Cleary, D W King and R A W Haddon: "P Wave Scattering in the Earth's Crust". Geophys J R Astr Soc, 43, 861-872 (1975)

9. M Båth: "The Elastic Waves Lg and Rg along Euro-Asiatic Paths". Arkiv fur Geophysik, 2, 295-342 (1954)

10. J Oliver and M Ewing: "Higher Modes of Continental Rayleigh Waves". Bull Seis Soc Am, 47, 187-204 (1957)

TABLE 1

$\overline{C}_{ij}$ for 28 October 1975 NTS/YKA

Channel Number	$\overline{C}_{ij}$	Upper Bound $\overline{C}_{ij}$	Lower Bound $\overline{C}_{ij}$	Number of Measurements	Distance from CG, km	Azimuth from CG, km
1	0.93823	0.98677	0.89411	62	14.56942	267.68213
2	0.94227	0.98864	0.90626	62	12.22916	267.18555
3	0.93691	0.98593	0.89031	61	9.82270	266.47705
4	0.92903	0.98278	0.87824	58	7.60863	264.88477
5	0.94338	0.98927	0.89633	61	5.81119	262.35962
6	0.94835	0.99009	0.91667	60	4.39285	250.41597
7	0.94194	0.98529	0.90163	60	4.39285	118.74658
9	0.93410	0.98013	0.88550	60	6.94570	95.18893
10	0.90099	0.97449	0.83057	55	9.05608	93.66580
11	0.95284	0.98780	0.91943	62	12.03033	162.04376
12	0.95252	0.98404	0.92430	61	9.57400	157.07056
13	0.95568	0.99024	0.91898	62	7.60864	147.85205
14	0.93008	0.97865	0.88362	62	6.21243	130.87624
15	0.86174	0.98738	0.78929	25	5.38011	98.84309
17	0.89169	0.98471	0.78924	57	7.28470	37.10170
18	0.90587	0.98395	0.83326	61	8.78568	26.16330
19	0.90939	0.99139	0.84216	58	10.53365	20.40439
20	0.84512	0.98930	0.75588	51	13.17850	16.03606

TABLE 2

$\overline{C}_{ij}$ for NTS Marsilly 5 April 1977/YKA

Channel Number	$\overline{C}_{ij}$	Upper Bound $\overline{C}_{ij}$	Lower Bound $\overline{C}_{ij}$	Number of Measurements	Distance from CG, km	Azimuth from CG, km
1	0.93098	0.98026	0.87870	49	14.73405	267.05811
2	0.91234	0.96603	0.85981	50	12.03030	266.41943
3	0.95832	0.99352	0.92942	50	9.82270	265.48291
4	0.90887	0.98217	0.83486	50	7.60863	263.48096
5	0.92581	0.96476	0.89111	50	5.81119	259.96436
6	0.94962	0.98130	0.91980	50	4.39285	243.40285
7	0.96037	0.98753	0.93128	50	4.39285	121.34119
10	0.56897	0.75738	0.37682	28	9.31863	94.57176
11	0.94532	0.98093	0.90981	50	12.03033	161.58072
12	0.95461	0.98919	0.92729	50	9.57400	156.59233
13	0.95457	0.98967	0.92188	50	7.91932	147.47191
14	0.95136	0.99001	0.91450	50	6.58927	131.06792
15	0.95428	0.99707	0.93975	22	5.81119	100.75604
16	0.82943	0.99076	0.60565	14	5.81118	62.07974
17	0.87880	0.98163	0.75809	36	7.28470	39.13440
18	0.86698	0.92807	0.80510	41	8.78568	27.57529
19	0.85887	0.96663	0.74524	43	10.53365	21.46201
20	0.83700	0.93957	0.73456	41	13.17850	16.85402

TABLE 3

$\overline{C_{ij}}$ for Utah Earthquake 29 March 1975/YKA

Channel Number	$\bar{C}_{ij}$	Upper Bound $\bar{C}_{ij}$	Lower Bound $\bar{C}_{ij}$	Number of Measurements	Distance from CG, km	Azimuth from CG, km
1	0.57679	0.82510	0.31556	37	15.37495	267.65601
2	0.67923	0.85214	0.49757	48	12.61749	267.17407
4	0.81221	0.91549	0.70873	52	8.21825	265.02490
5	0.81350	0.94662	0.67037	52	6.21242	262.87012
6	0.88819	0.94794	0.83063	53	4.39285	254.48135
7	0.89300	0.95561	0.82693	54	4.39285	142.27359
9	0.89139	0.96718	0.82728	53	6.94570	96.01671
10	0.83958	0.94438	0.73712	52	9.05608	94.14284
11	0.90888	0.96696	0.85154	53	11.82813	164.70703
12	0.92661	0.96772	0.88470	51	9.31865	160.37030
13	0.93318	0.97876	0.89703	46	7.60864	152.10884
14	0.91294	0.96369	0.86073	45	6.21243	135.90440
15	0.88325	0.94599	0.81855	20	4.91135	101.00679
17	0.90025	0.97274	0.83703	45	7.28470	32.81323
18	0.83743	0.96529	0.70755	52	8.50669	22.70738
19	0.90854	0.95337	0.86489	48	10.53365	17.59874
20	0.81510	0.92312	0.71192	44	12.99417	13.72072

TABLE 4

$\overline{C_{ij}}$ for 7 April 1975 Queen Charlotte Is/YKA

Channel Number	$\bar{C}_{ij}$	Upper Bound $\bar{C}_{ij}$	Lower Bound $\bar{C}_{ij}$	Number of Measurements	Distance from CG, km	Azimuth from CG, km
1	0.74175	0.86484	0.61318	25	14.73405	267.05298
2	0.80641	0.88008	0.73087	25	12.22916	266.37646
3	0.87306	0.95250	0.79348	22	9.82270	265.45190
4	0.79888	0.92227	0.66319	27	8.21825	263.34155
5	0.80874	0.94384	0.66258	27	6.21242	259.69751
6	0.85910	0.93578	0.78048	27	4.91135	241.12555
7	0.82796	0.90187	0.75427	27	4.91135	118.26323
9	0.85798	0.91412	0.80041	16	7.91931	96.27089
11	0.70759	0.83599	0.57302	26	12.22919	160.92619
12	0.75768	0.89764	0.60738	24	10.06529	155.82867
13	0.81538	0.93796	0.68941	23	8.21827	146.48061
14	0.90934	0.95594	0.85928	27	6.94570	129.97379
15	0.87542	0.93783	0.81367	24	6.21242	100.36790
16	0.82940	0.91886	0.73532	20	6.58926	62.94064
17	0.88288	0.96351	0.79314	25	7.60862	40.14191
18	0.83953	0.95006	0.73621	27	9.05606	28.42780
19	0.84752	0.95496	0.74556	25	10.76021	22.16376
20	0.82560	0.95598	0.69182	24	13.17850	17.43863

TABLE 5

$\overline{C_{ij}}$ for Alaskan Earthquake 9 March 1975/YKA

Channel Number	$\bar{C}_{ij}$	Upper Bound $\overline{Cij}$	Lower Bound $\bar{C}_{ij}$	Number of Measurements	Distance from CG, km	Azimuth from CG, km
1	0.81813	0.94102	0.70006	25	14.56942	267.02832
2	0.83324	0.93517	0.73171	25	12.03030	266.37354
3	0.84414	0.94710	0.74244	24	9.82270	265.41235
4	0.88060	0.97307	0.78565	18	7.91931	263.34106
5	0.91844	0.94508	0.89118	18	5.81119	259.61548
6	0.89982	0.96328	0.84106	21	4.91135	240.96042
7	0.95837	0.99030	0.92930	20	4.91135	118.52551
9	0.82350	0.90440	0.74656	13	7.60863	96.27347
11	0.81429	0.93225	0.69486	23	12.22919	160.94917
12	0.89497	0.96920	0.83388	22	9.82272	155.82451
13	0.93184	0.97702	0.88516	24	8.21827	146.53108
14	0.89733	0.95487	0.83857	24	6.58927	130.05087
15	0.80289	0.94008	0.66620	15	5.81119	100.37611
16	0.89840	0.96093	0.83556	24	6.21242	62.92416
17	0.84104	0.92907	0.75585	21	7.60862	40.15285
18	0.72738	0.82238	0.62983	23	9.05606	28.42807
19	0.88368	0.96941	0.78502	15	10.76021	22.16078
20	0.77779	0.87606	0.67636	16	13.17850	17.43700

TABLE 6

$\overline{C_{ij}}$ for Vancouver Is 1 January 1976/YKA

Channel Number	$\bar{C}_{ij}$	Upper Bound $\bar{C}_{ij}$	Lower Bound $\bar{C}_{ij}$	Number of Measurements	Distance from CG, km	Azimuth from CG, km
1	0.74416	0.89285	0.59613	35	15.05791	267.30103
2	0.76539	0.92624	0.60384	45	12.61749	266.72827
3	0.81630	0.94459	0.68772	45	10.06527	265.90796
4	0.82419	0.91535	0.73400	49	8.21825	264.15161
5	0.89784	0.96057	0.83514	52	5.81119	261.29541
6	0.92519	0.96320	0.88624	53	4.91135	249.25266
7	0.91204	0.97036	0.85419	53	4.91135	128.92691
9	0.86112	0.96172	0.76013	32	7.28471	96.35538
10	0.86155	0.93630	0.78415	51	9.31863	94.46271
11	0.88941	0.98105	0.80644	51	12.03033	163.08348
12	0.90615	0.97707	0.83430	51	9.57400	158.40305
13	0.90086	0.98868	0.79190	53	7.60864	149.68510
14	0.91707	0.98442	0.86277	50	6.58927	133.36499
15	0.91519	0.99019	0.84892	52	5.38011	101.08263
16	0.74510	0.84271	0.64616	44	5.81118	59.25336
17	0.91985	0.97140	0.86093	52	7.28470	36.26207
18	0.81863	0.91507	0.71635	53	9.05606	25.30276
19	0.73138	0.87524	0.57902	52	10.53365	19.63896
20	0.65330	0.83115	0.46928	44	12.99417	15.36735

TABLE 7

$\overline{C_{ij}}$ for Kashmir 11 December 1975/GBA

Channel Number	$\bar{C}_{ij}$	Upper Bound $\bar{C}_{ij}$	Lower Bound $\bar{C}_{ij}$	Number of Measurements	Distance from CG, km	Azimuth from CG, km
1	0.91662	0.95747	0.87455	20	4.92346	72.12711
2	0.87538	0.93949	0.81186	20	3.81369	40.41376
3	0.91181	0.94262	0.87906	20	4.40368	4.47541
4	0.83511	0.88681	0.78167	20	5.82551	341.63647
5	0.81743	0.94478	0.68285	20	7.62739	331.48755
6	0.83912	0.93196	0.74673	18	9.84691	324.72119
7	0.64833	0.86000	0.41999	20	12.45547	319.96484
11	0.82695	0.96209	0.66386	20	5.82552	81.57861
12	0.93422	0.95879	0.90917	20	4.40368	103.13748
13	0.92779	0.97019	0.88204	20	4.40368	139.97476
14	0.86603	0.92443	0.80584	20	5.82552	161.76935
15	0.75585	0.93445	0.57077	20	7.62740	177.36092
16	0.61513	0.73957	0.48785	20	9.84693	185.02544
17	0.83816	0.88817	0.78630	13	12.25934	189.83728

TABLE 8

$\overline{C_{ij}}$ for Tibet 3 October 1976/GBA

Channel Number	$\bar{C}_{ij}$	Upper Bound $\bar{C}_{ij}$	Lower Bound $\bar{C}_{ij}$	Number of Measurements	Distance from CG, km	Azimuth from CG, km
1	0.91814	0.93617	0.90002	18	4.92346	82.85963
2	0.89255	0.93605	0.84898	18	3.11387	50.20544
3	0.78358	0.84127	0.72464	18	3.11387	3.02333
4	0.78470	0.86401	0.70357	18	4.40368	336.36816
5	0.84212	0.93939	0.73485	18	6.96282	326.81128
6	0.90022	0.97655	0.82986	18	9.59758	320.60156
7	0.80701	0.91829	0.68954	18	11.85725	316.55859
11	0.81138	0.90858	0.71233	18	5.82552	90.66183
12	0.74415	0.86097	0.62087	18	4.92346	115.00327
13	0.90724	0.96301	0.84450	18	4.92346	147.90953
14	0.88969	0.95199	0.81796	18	6.96283	165.50087
15	0.81131	0.92092	0.70173	18	8.23853	178.74231
16	0.90083	0.95622	0.84596	18	10.55966	185.44853

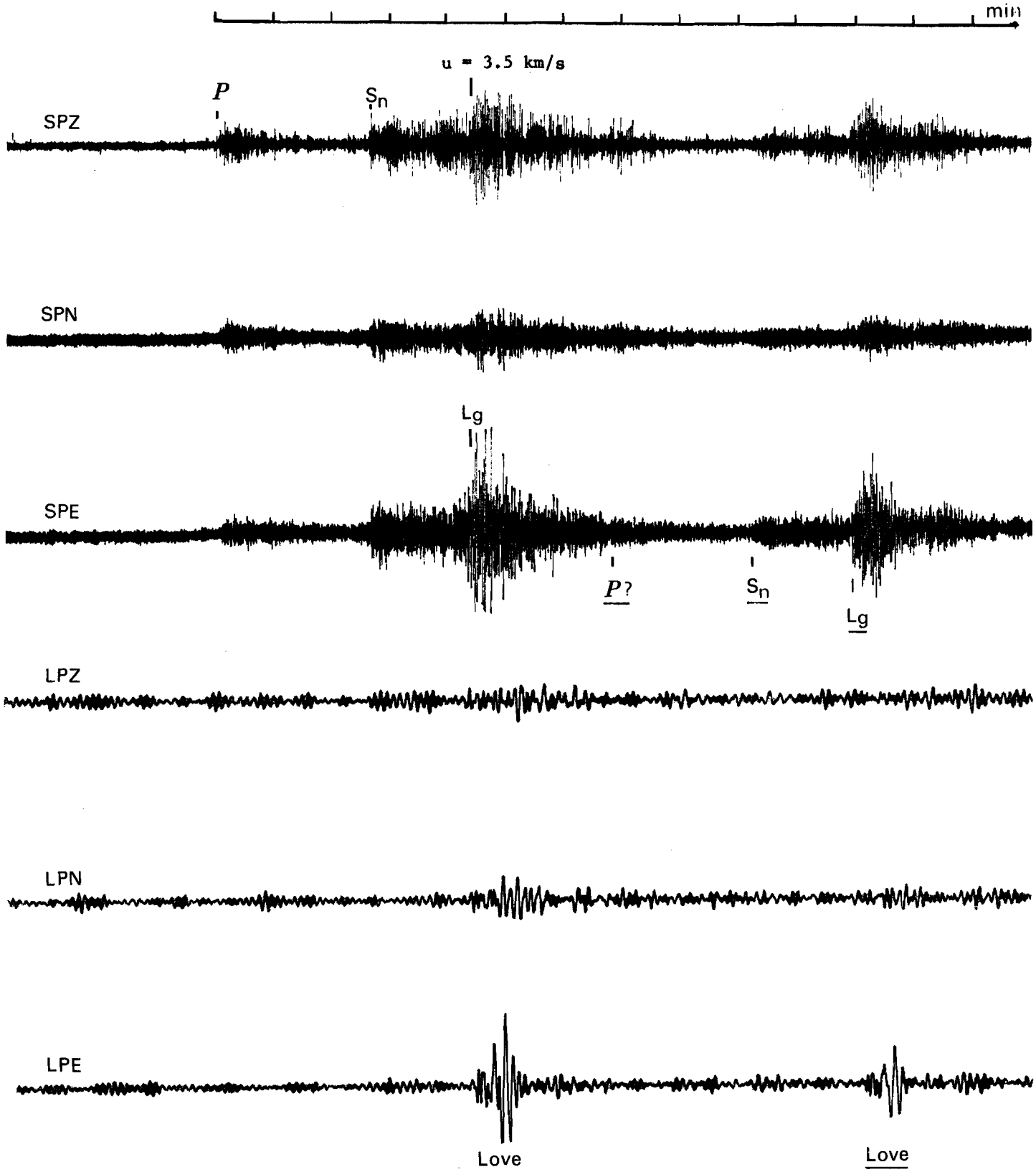

FIGURE 1. ILLUSTRATES THREE COMPONENT SETS OF SHORT AND LONG PERIOD SEISMOGRAMS FOR TWO EARTHQUAKES ALMOST COINCIDENT IN SPACE AND TIME

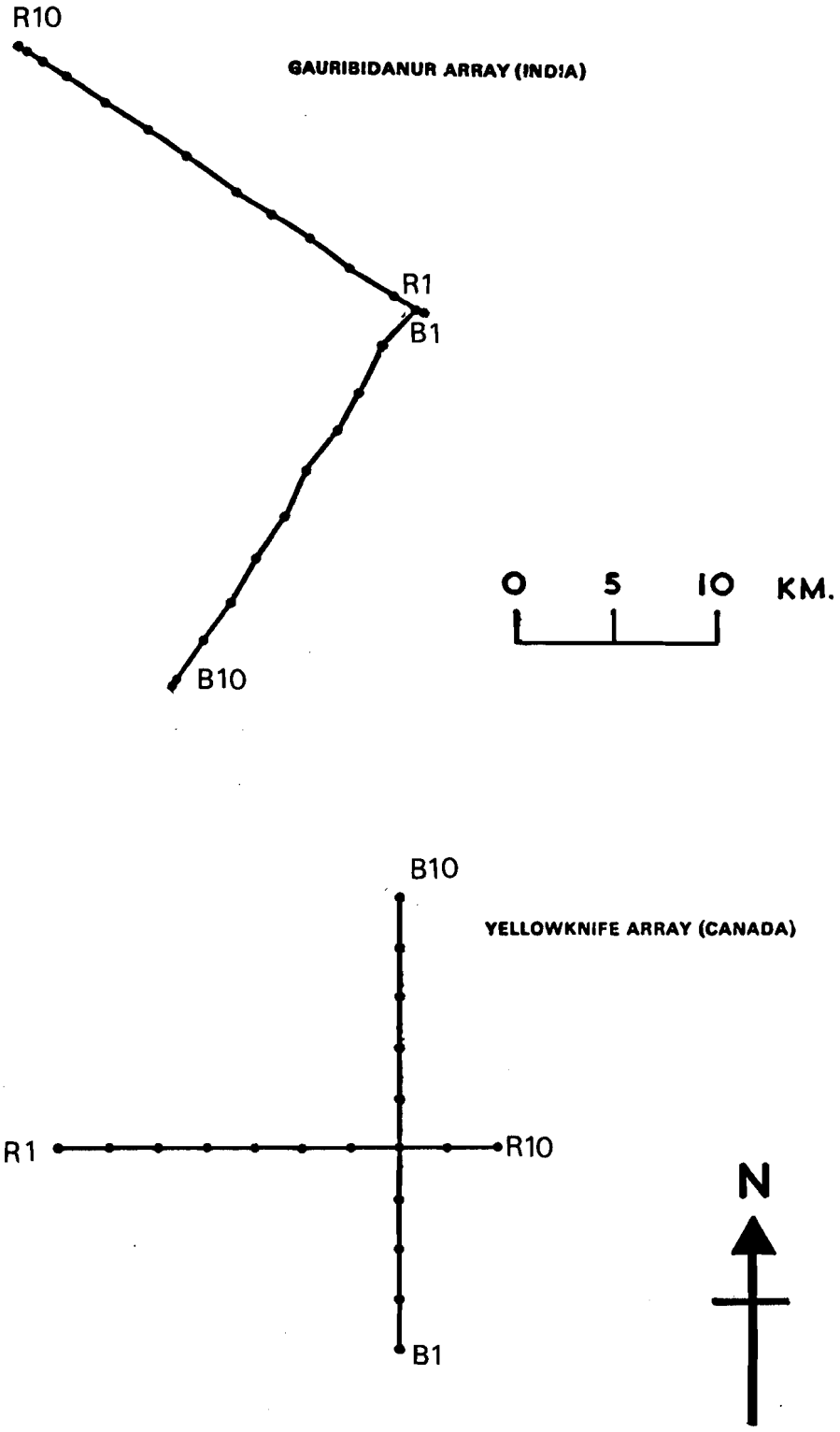

FIGURE 2. THE LAYOUT AND SCALE OF THE GBA AND YKA ARRAY STATIONS

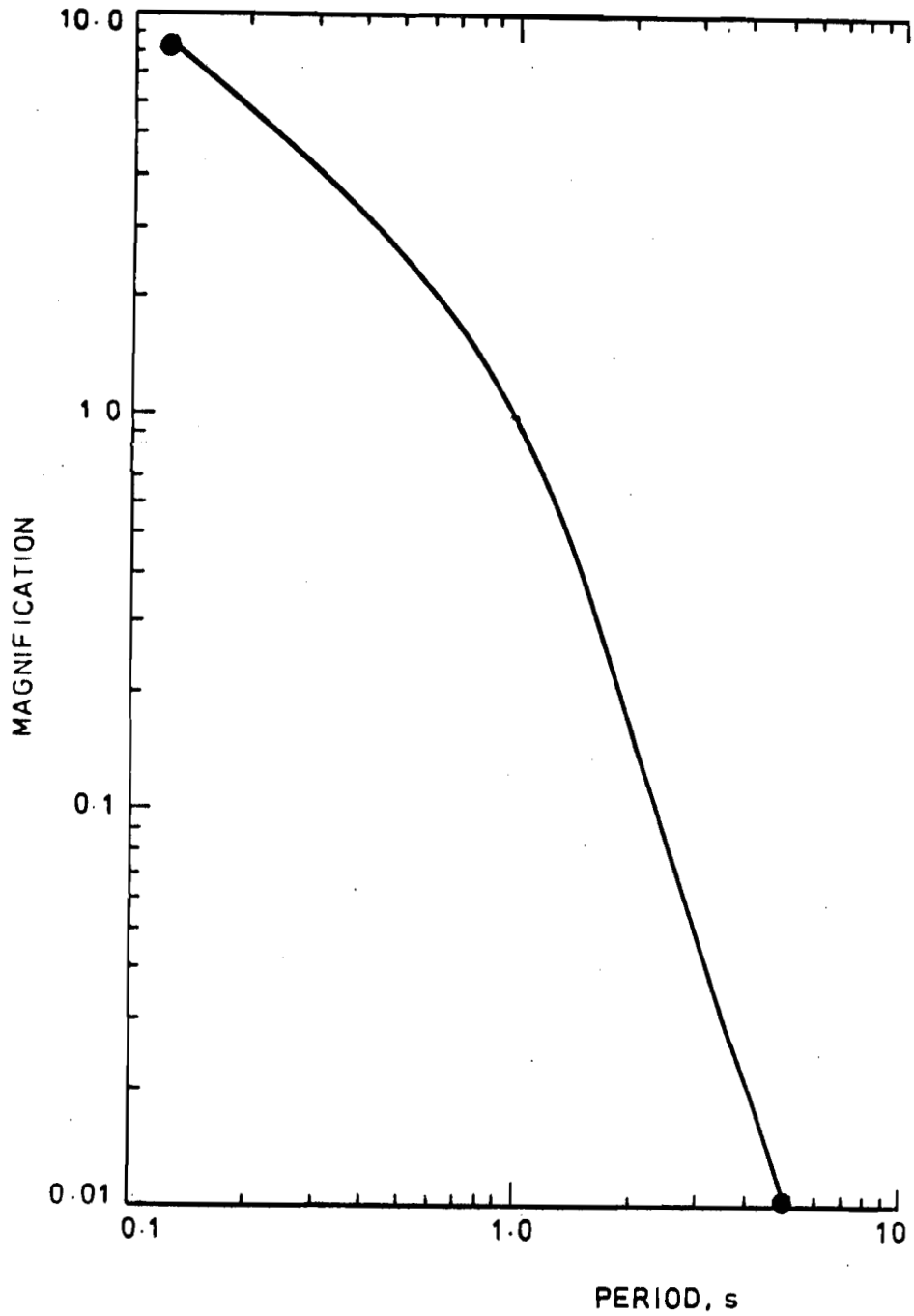

FIGURE 3. THE FREQUENCY RESPONSE OF THE SHORT PERIOD SEISMOMETERS USED TO PROVIDE THE DATA FOR THIS REPORT

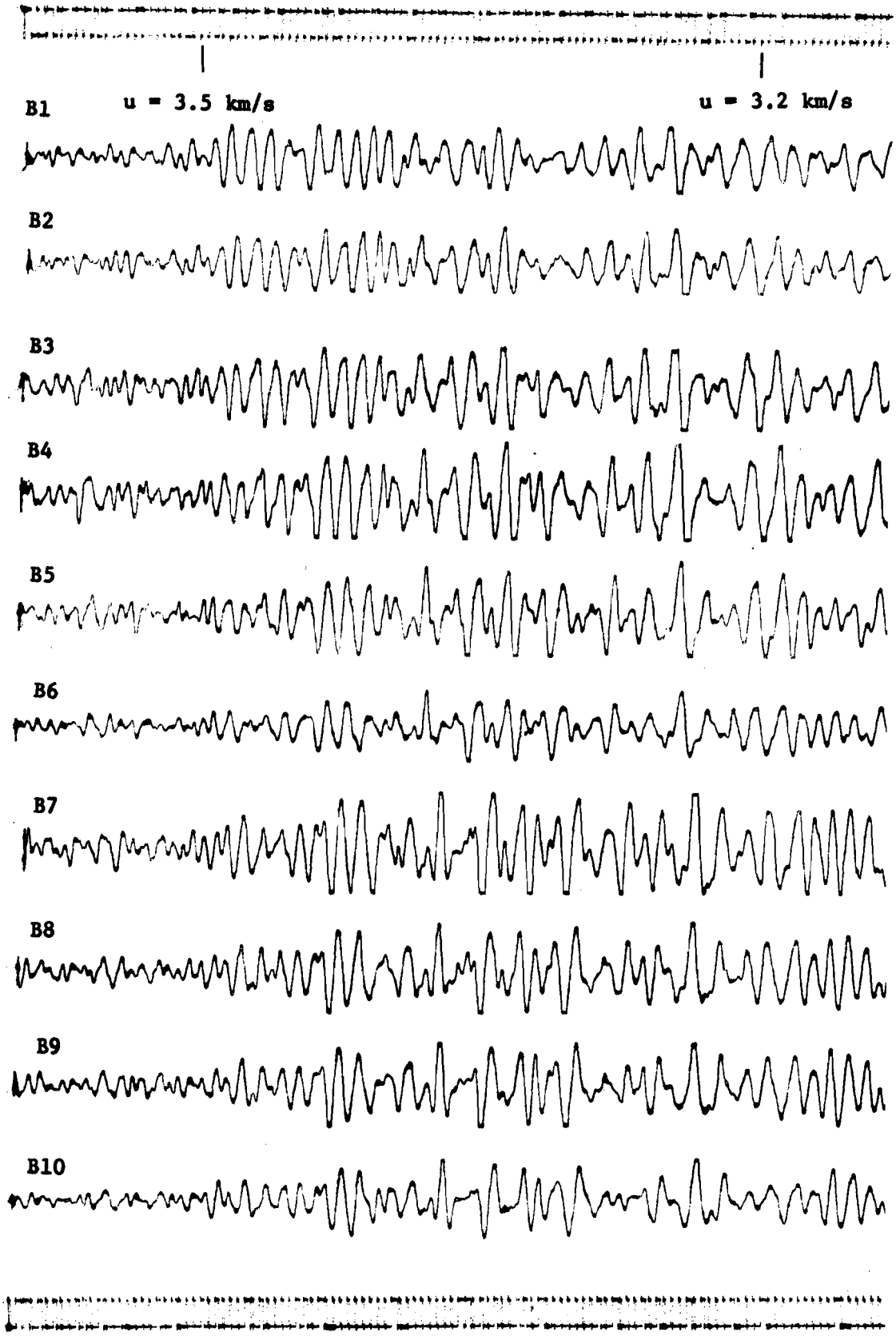

FIGURE 4. AN ILLUSTRATION OF AN R_1 WAVETRAIN REPRESENTING A MIXTURE OF MODES EACH WITH ITS OWN PHASE VELOCITY

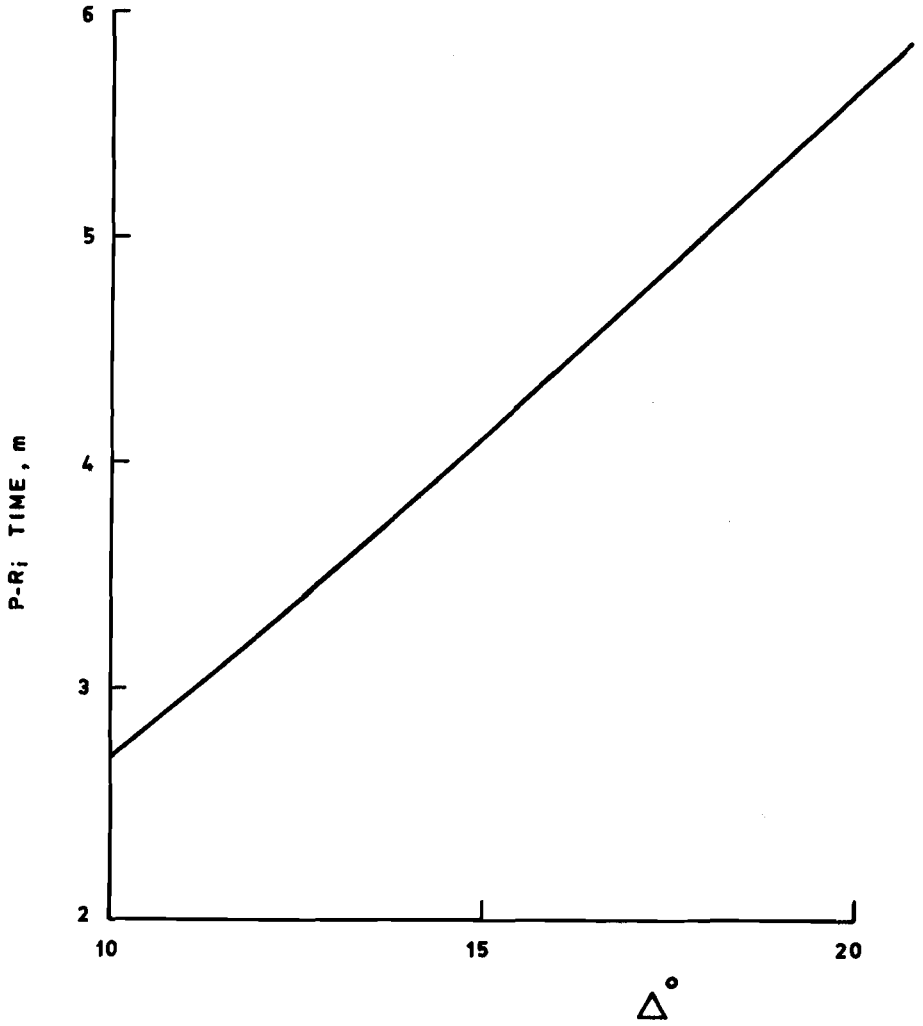

FIGURE 5. P-R_i Time as a Function of Δ, for Group Velocity $U(R_i) = 3.6$ km/s, J-B Travel Times for P

ANNEX TO FIGURE 6

Source: Explosion

Region: Nevada Test Site/YKA

Date: 28 October 1975

Origin Time: 14-30-00.0

Latitude: 37.12N

Longitude: 116.06W

Depth: < 1 km

m_b: 6.4

Known Back Bearing: N183°E

Estimated: N177.89 ± 0.01°E

Known Δ: 25.3°

$(R_i - P)$ Time: 7 min 56 s

Estimated Δ $(R_i - P)$: 26.2°

Tangential Error: 248.0 km

Radial Error: 100.0 km

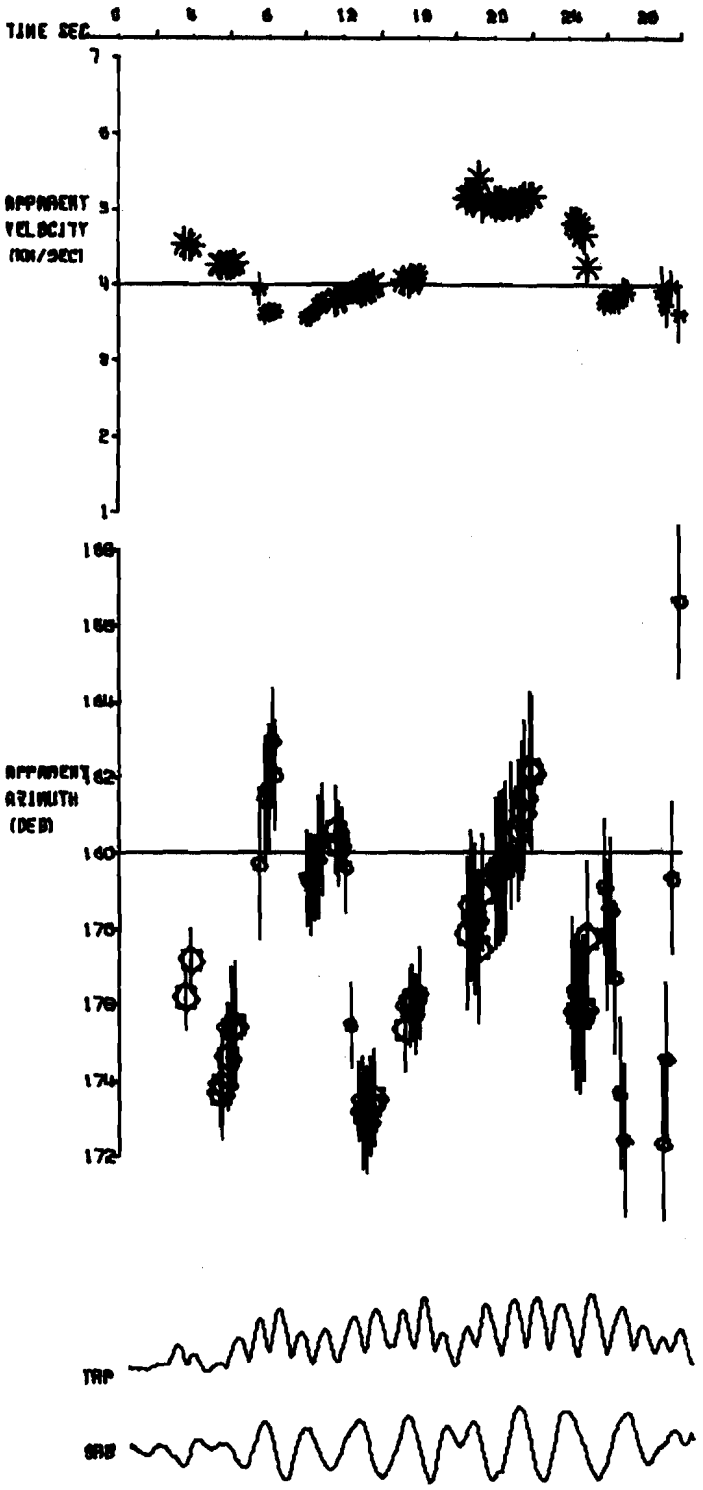
TIME SEC
APPARENT VELOCITY (KM/SEC)
APPARENT AZIMUTH (DEG)
TRP
BRB

FIGURE 6

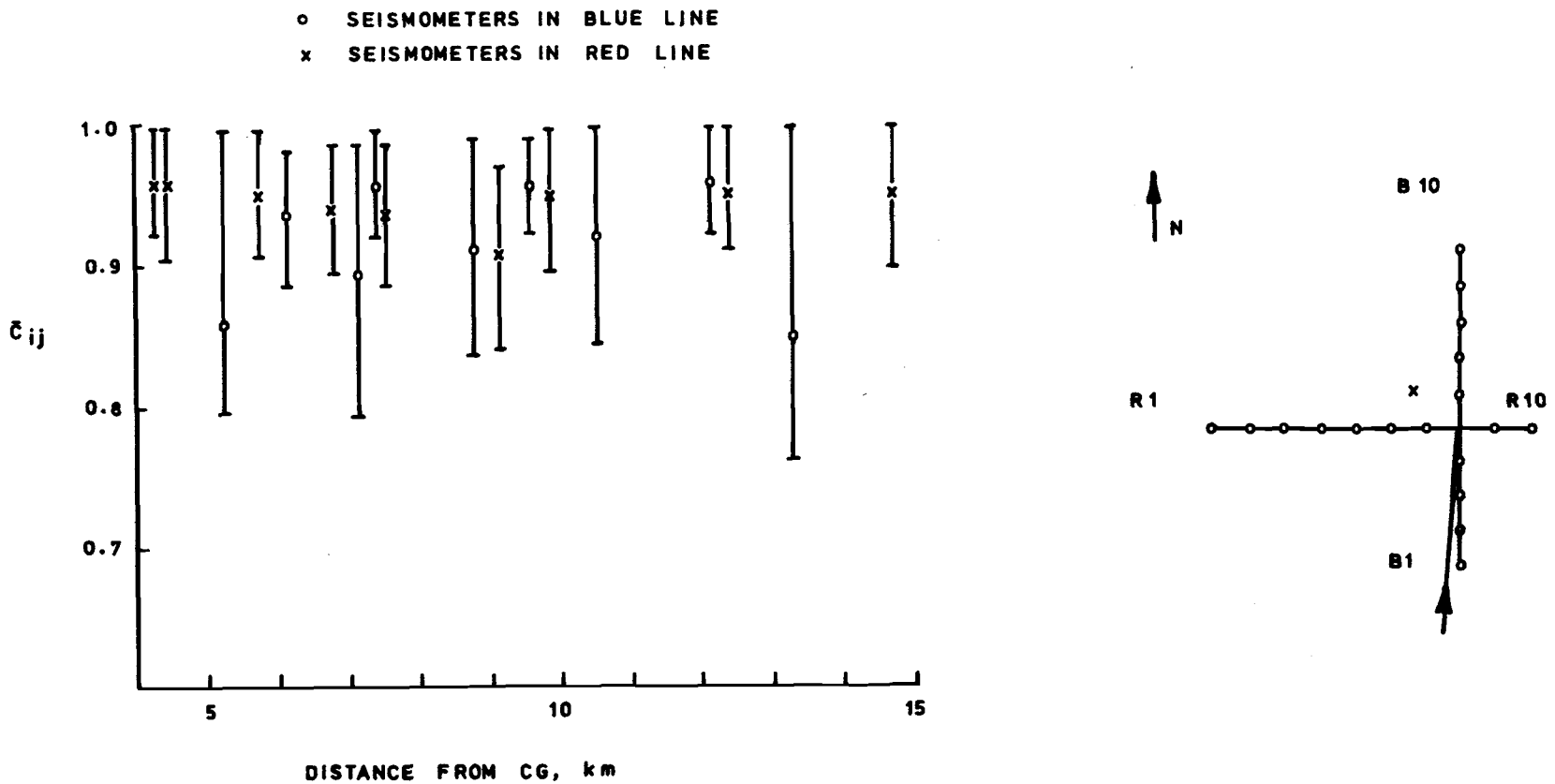

FIGURE 7. $\bar{C}_{ij}$ as a Function of Distance from the Centre of Gravity (CG) of the YKA array for the NTS explosion of 28 October 1975. A Diagram of the array layout is given on the right of the plot and shows the Centre of Gravity (CG) of the array and an arrow indicating the Signal Azimuth.

ANNEX TO FIGURE 8

Source: Explosion

Region: NTS/YKA

Date: 5 April 1977

Origin Time: 15-00-00.0

Latitude: 37.12N

Longitude: 116.06W

Depth: < 1 km

m_b: 5.4

Known Back Bearing: N183°E

Estimated: N180.76 ± 0.003°E

Known Δ: 25.3°

$(R_i - P)$ Time: 7 min 50 s

Estimated Δ $(R_i - P)$: 25.8°

Tangential Error: 108 km

Radial Error: 55 km

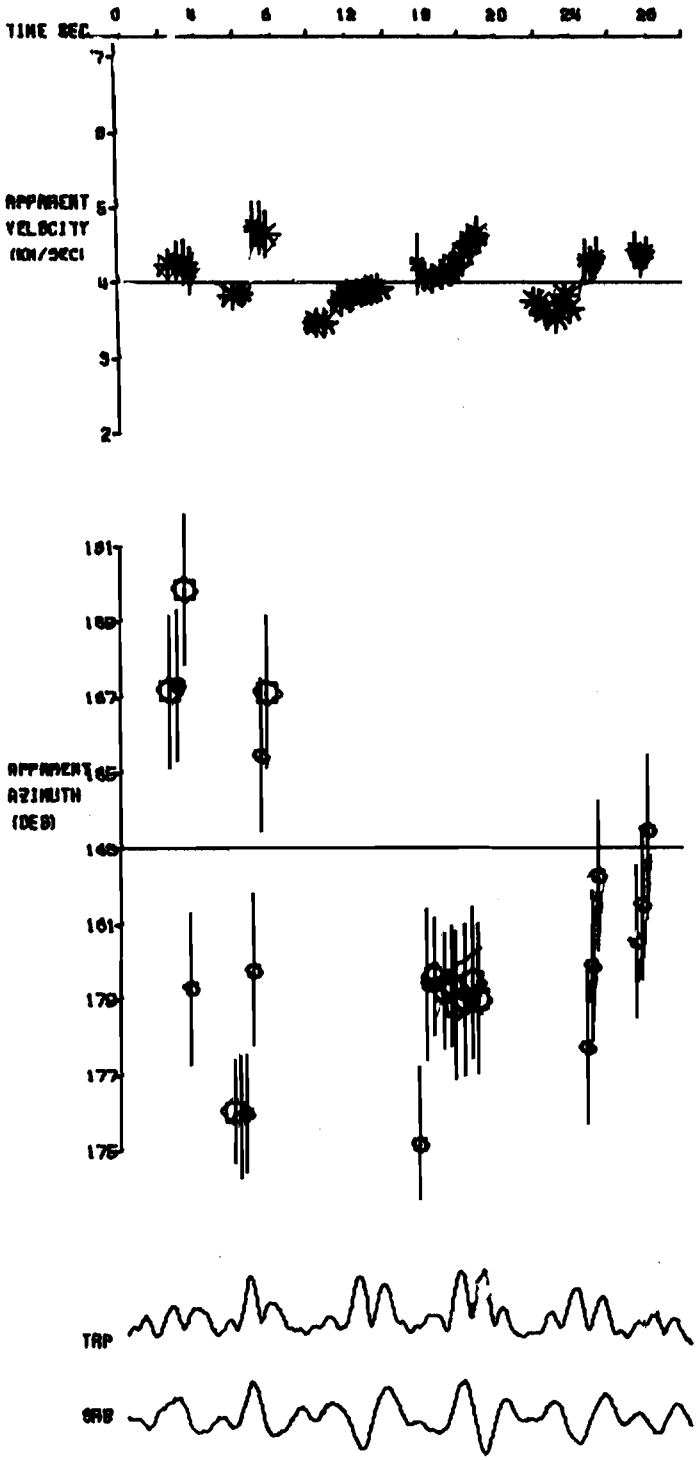
TIME SEC
0
6
12
18
20
24
30
APPARENT VELOCITY (KM/SEC)
7
6
5
4
3
2
APPARENT AZIMUTH (DEG)
181
169
167
165
161
179
177
175
TRP
SRB

FIGURE 8

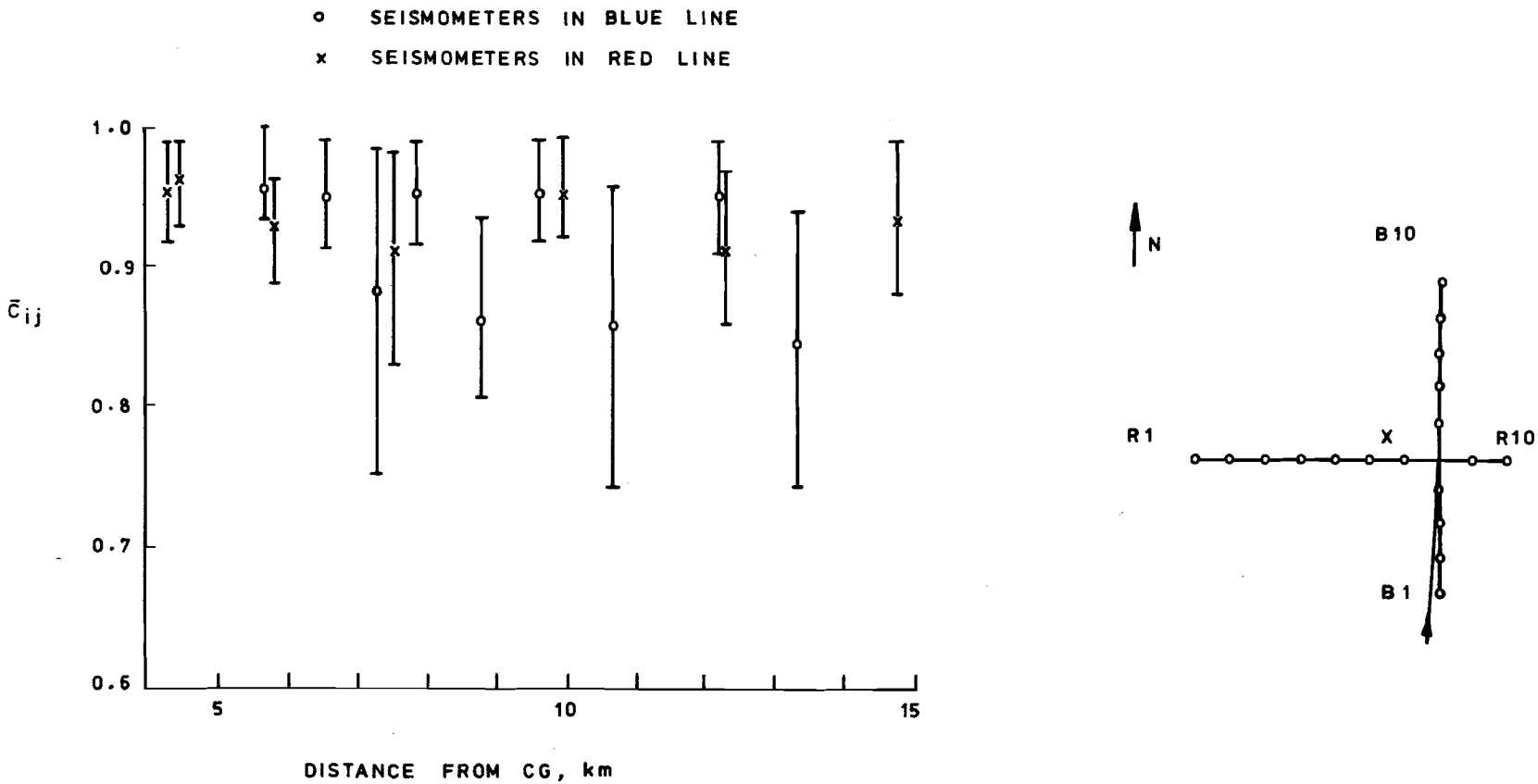

FIGURE 9. $\bar{C}_{ij}$ as a Function of Distance from the Centre of Gravity (CG) of the YKA array for the NTS Marsilly explosion of 5 April 1977. A Diagram of the array layout is given on the right of the plot and shows the Centre of Gravity (CG) of the array and an arrow indicating the Signal Azimuth.

ANNEX TO FIGURE 10

Source: Earthquake

Region: Utah/YKA

Date: 29 March 1975

Origin Time: 13-01-23

Latitude: 41.92N

Longitude: 112.28W

Depth: 29 ± 13 km

Known Back Bearing: N175.4°E

Estimated: N175 ± N/A* °E

Known Δ: 20.3°

$(R_i - P)$ Time: 6 min 05 s

Estimated Δ $(R_i - P)$: 21.0°

Tangential Error: 5 km

Radial Error: 78 km

*N/A: Not available.

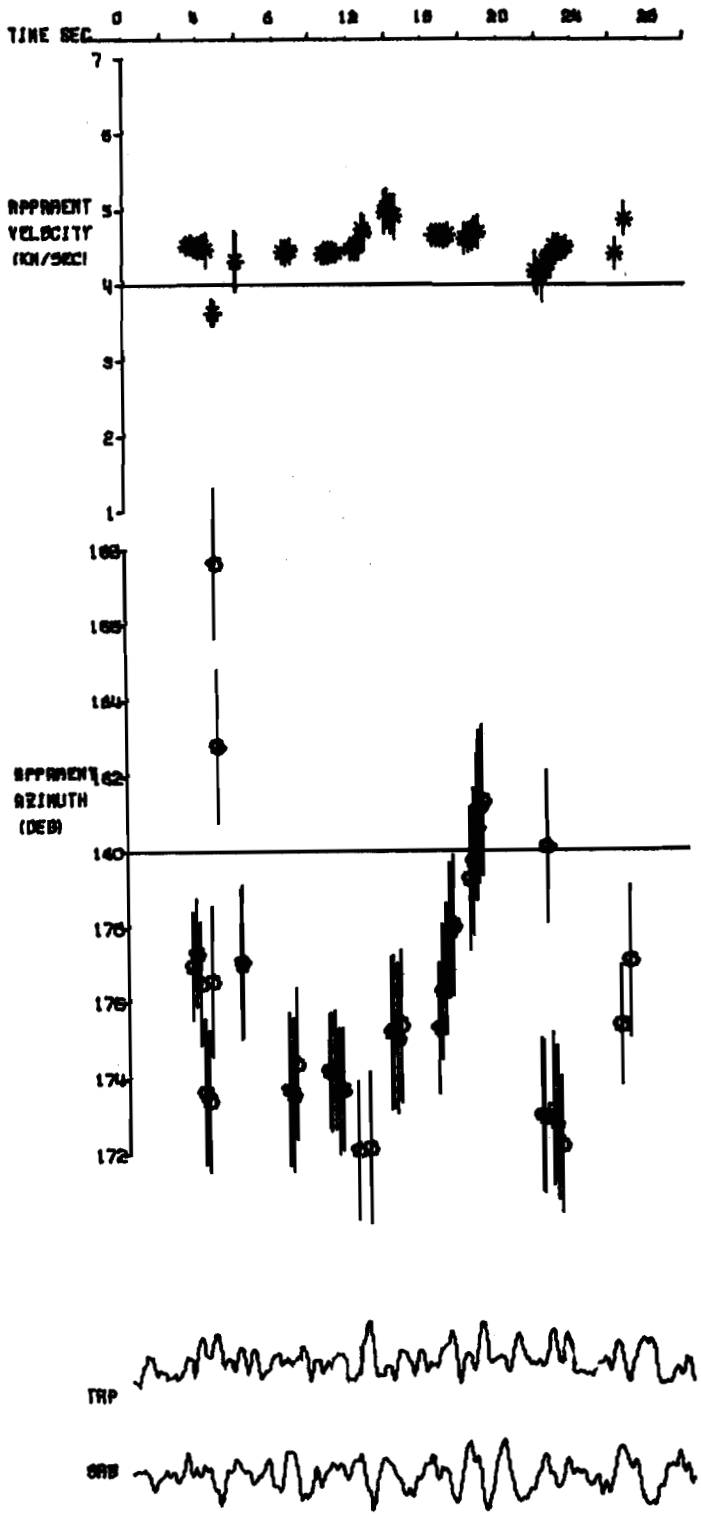
TIME SEC
0
6
12
18
24
APPARENT VELOCITY (KM/SEC)
7
6
5
4
3
2
1
APPARENT AZIMUTH (DEG)
140
175
174
172
TRP
BRB

FIGURE 10

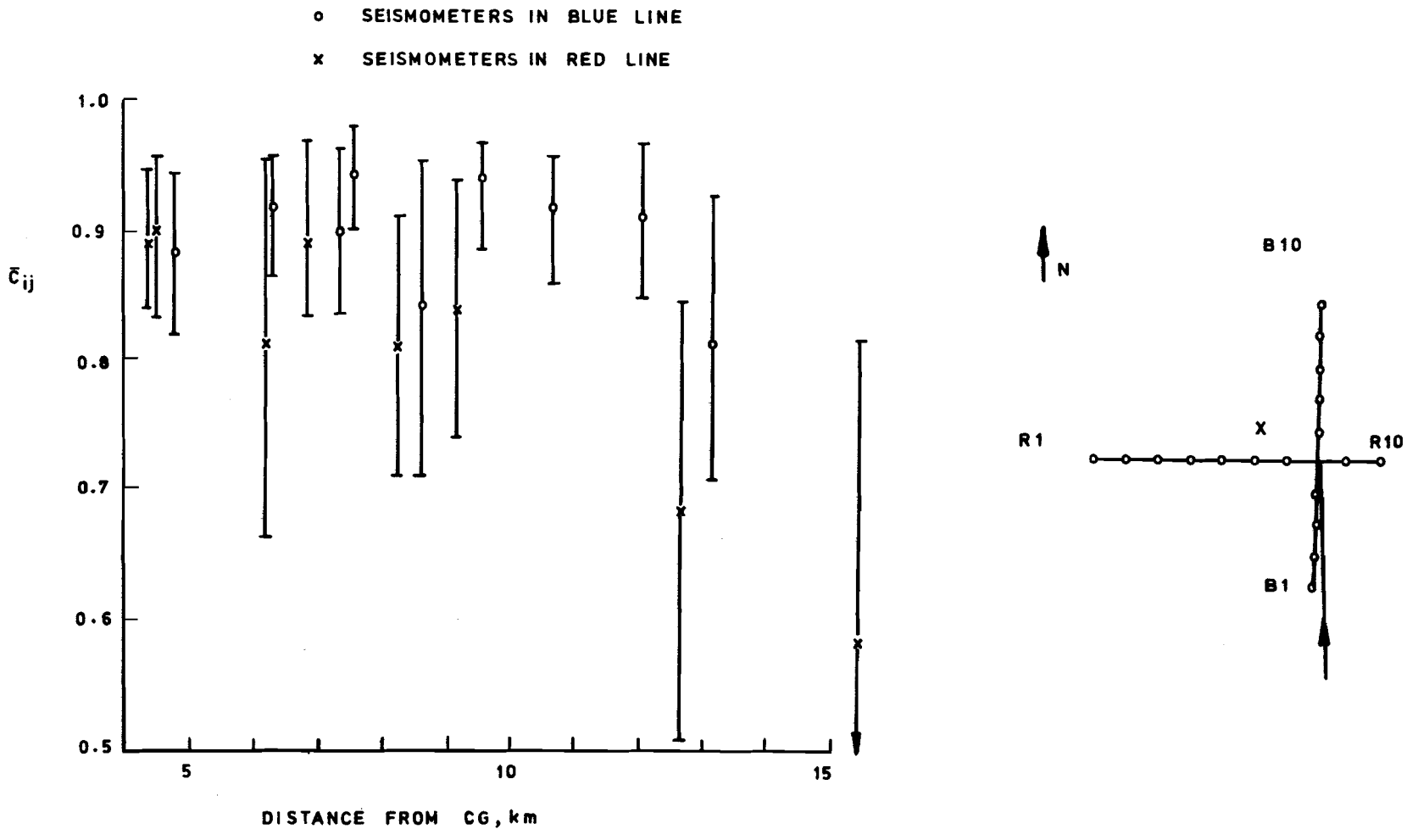

FIGURE 11. $\bar{C}_{ij}$ as a Function of Distance from the Centre of Gravity (CG) of the YKA array for the Utah earthquake of 29 March 1975. A Diagram of the array layout is given on the right of the plot and shows the Centre of Gravity (CG) of the array and an arrow indicating the Signal Azimuth.

ANNEX TO FIGURE 12

Source: Earthquake

Region: Queen Charlotte Is/YKA

Date: 7 April 1975

Origin Time: 01-47-47.0

Latitude: 52.01N

Longitude: 130.4W

Depth: 28 ± 34 km

Known Back Bearing: N225.1°E

Estimated: N218.34 ± 0.004°E

Known Δ: 13.6°

$(R_i - P)$ Time: 4 min 25 s

Estimated Δ $(R_i - P)$: 16.0°

Tangential Error: 180 km

Radial Error: 270 km

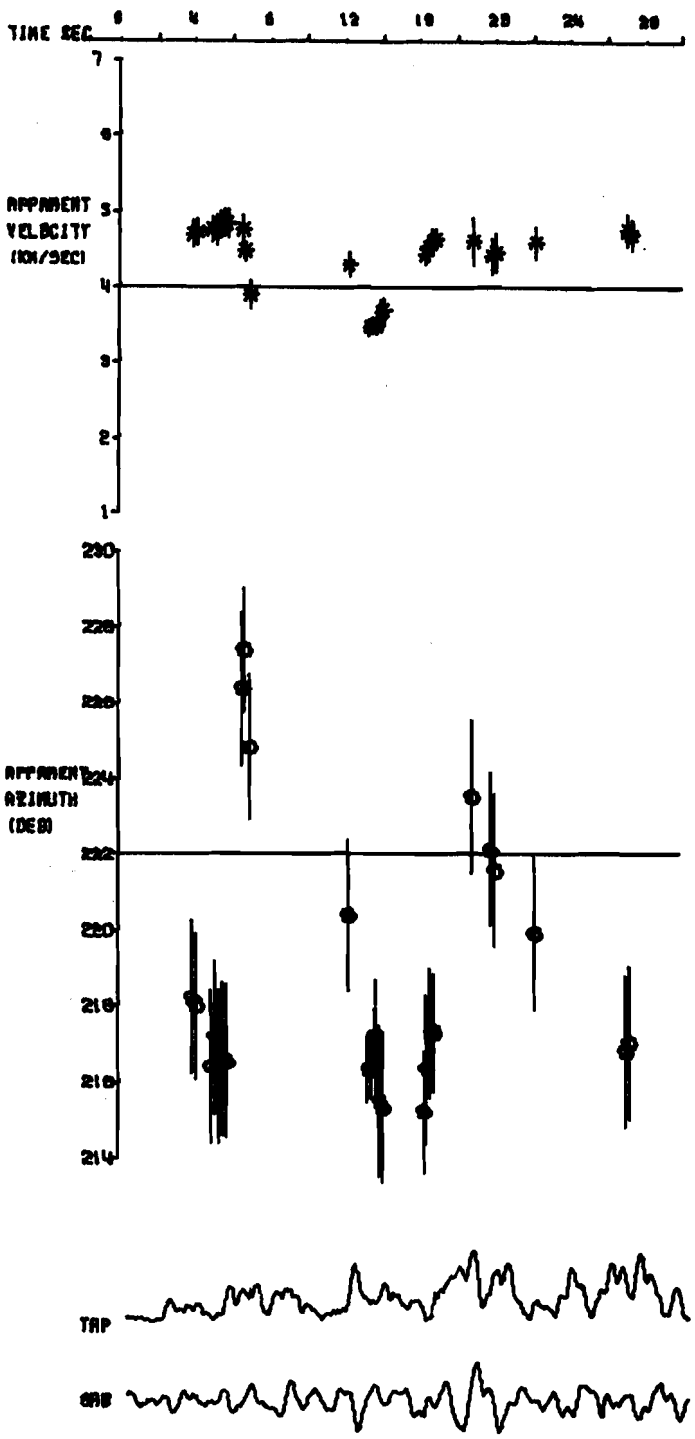
TIME SEC
0
4
8
12
16
20
24
28
APPARENT VELOCITY (KM/SEC)
7
6
5
4
3
2
1
APPARENT AZIMUTH (DEG)
230
228
226
224
222
220
218
216
214
TRP
BRB

FIGURE 12

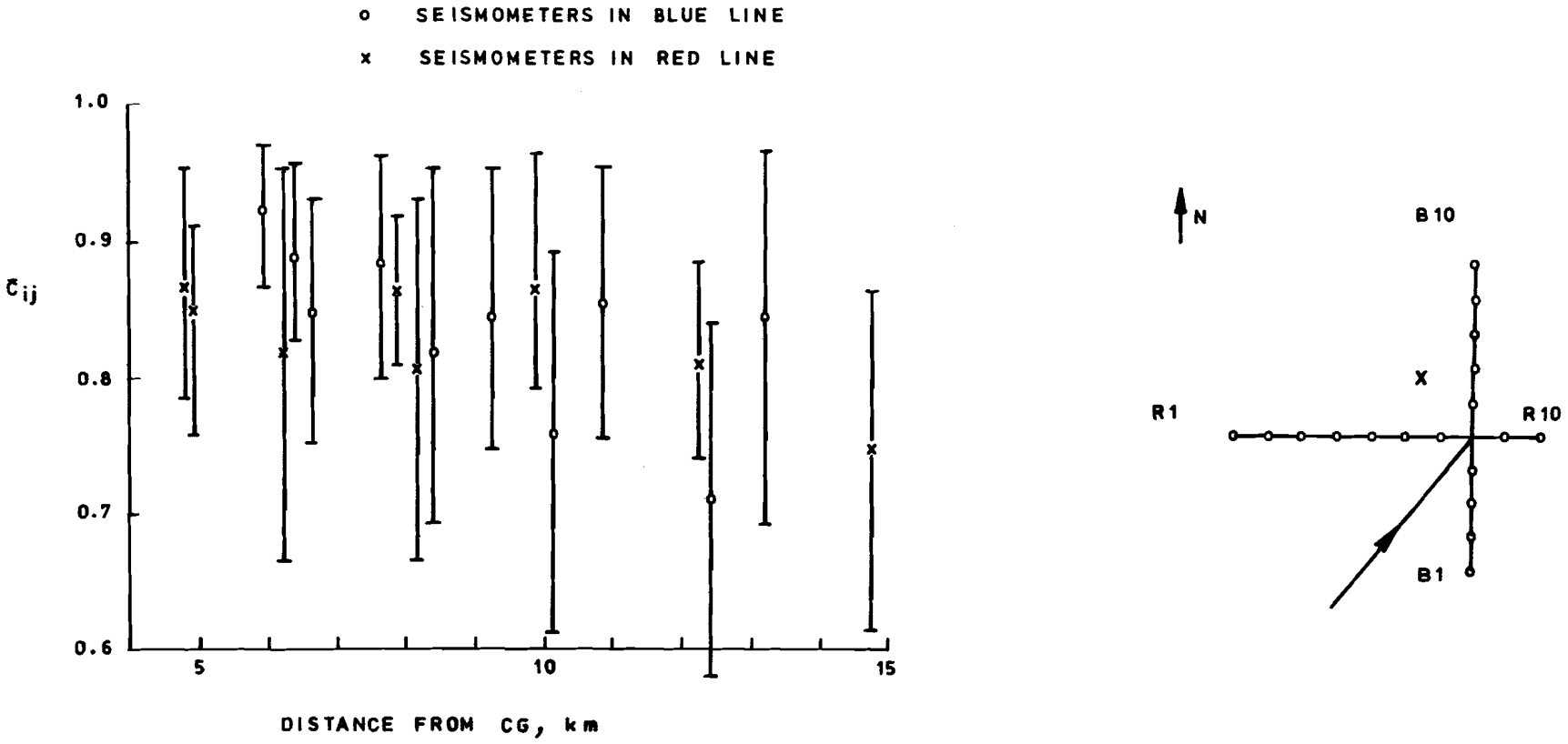

FIGURE 13. $\bar{C}_{ij}$ as a Function of Distance from the Centre of Gravity (CG) of the YKA array for the Queen Charlotte Isle earthquake of 7 April 1975. A Diagram of the array layout is given on the right of the plot and shows the Centre of Gravity (CG) of the array and an arrow indicating the Signal Azimuth.

ANNEX TO FIGURE 14

Source: Earthquake

Region: Alaska/YKA

Date: 9 March 1975

Origin Time: 14-19-41.9

Latitude: 65.92N

Longitude: 150.0W

Depth: 35 km

m_b: 3.8 ISC

Known Back Bearing: N297.8°E

Estimated: N296.1 ± 0.02°E

Known Δ: 15.60°

$(R_i - P)$ Time: 4 min 40 s

Estimated Δ $(R_i - P)$: 16.9°

Tangential Error: 52.0 km

Radial Error: 143 km

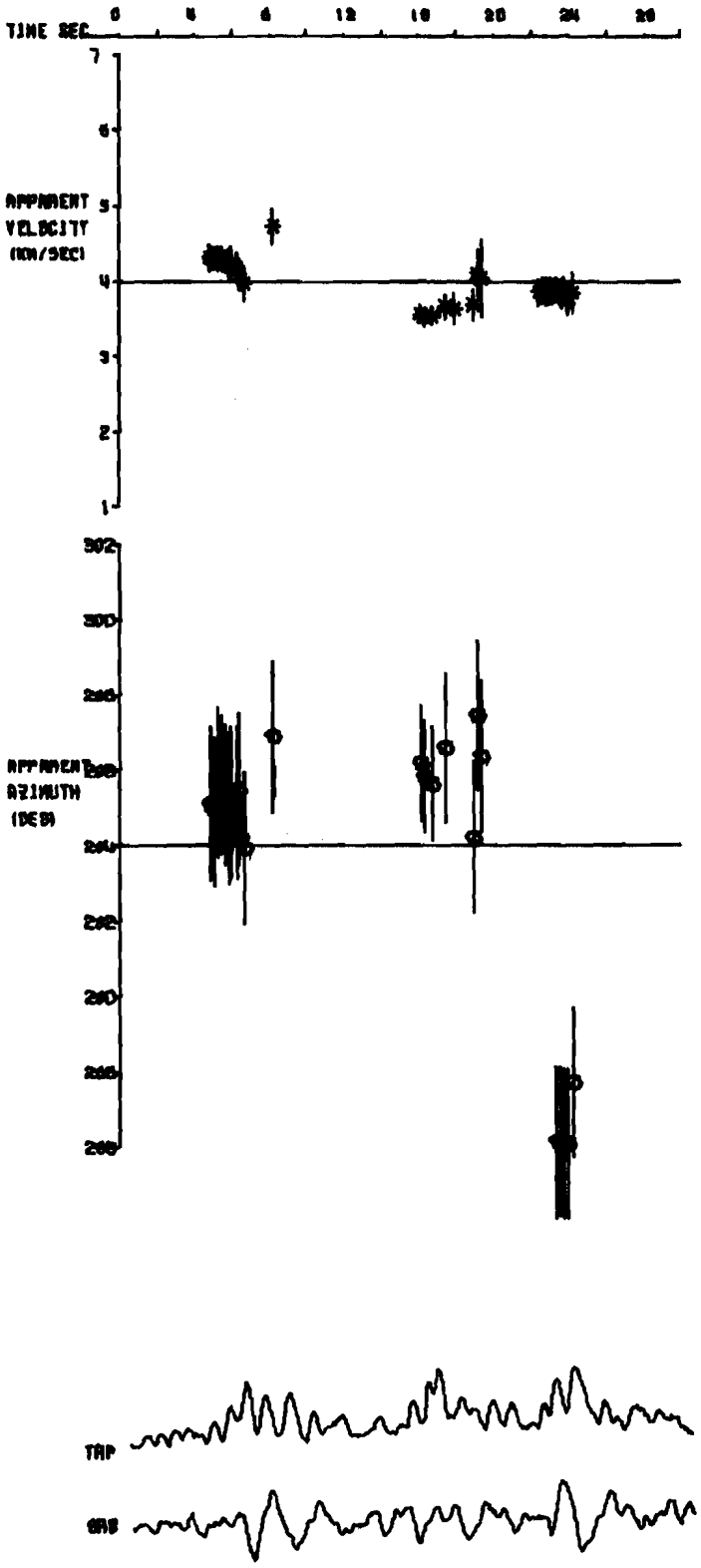
TIME SEC
0
4
8
12
16
20
24
28
APPARENT VELOCITY (KM/SEC)
7
6
5
4
3
2
1
APPARENT AZIMUTH (DEG)
302
300
298
296
294
292
290
288
286
TRP
GRB

FIGURE 14

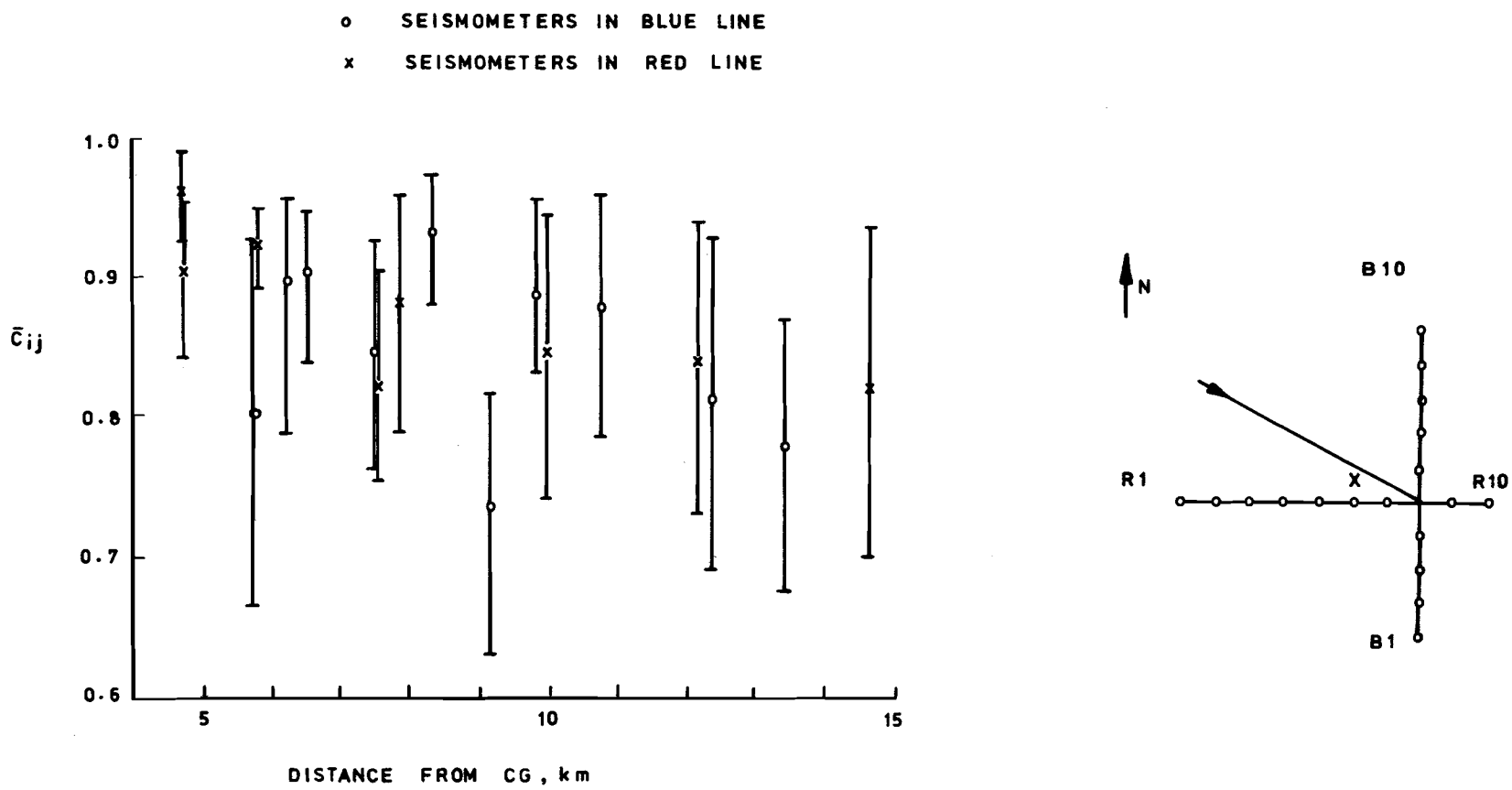

FIGURE 15. $\bar{C}_{ij}$ as a Function of Distance from the Centre of Gravity (CG) of the YKA array for the Alaskan earthquake of 9 March 1975. A Diagram of the array layout is given on the right of the plot and shows the Centre of Gravity (CG) of the array and an arrow indicating the Signal Azimuth.

ANNEX TO FIGURE 16

Source: Earthquake

Region: Vancouver Island

Date: 1 January 1976

Origin Time: 04-11-41.8

Latitude: 50.27N

Longitude: 129.82W

Depth: 19.0 km

m_b: 4.8

Known Back Bearing: N221.2°E

Estimated: N218.0 ± 0.01°E

Known Δ: 14.81°

(R_i - P) Time: 4 min 17 s

Estimated Δ (R_i - P): 15.5°

Tangential Error: 92 km

Radial Error: 77 km

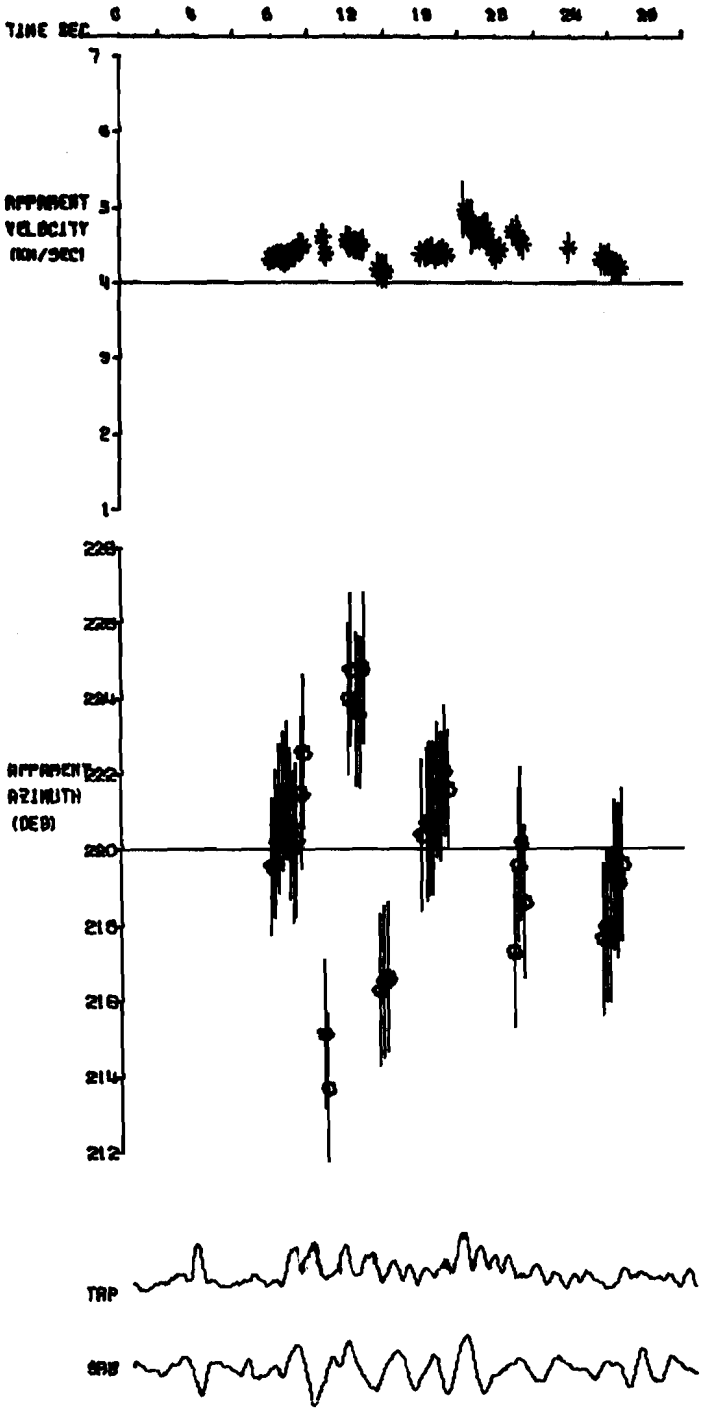
TIME SEC
APPARENT VELOCITY (KM/SEC)
APPARENT AZIMUTH (DEG)
TRP
SRB

FIGURE 16

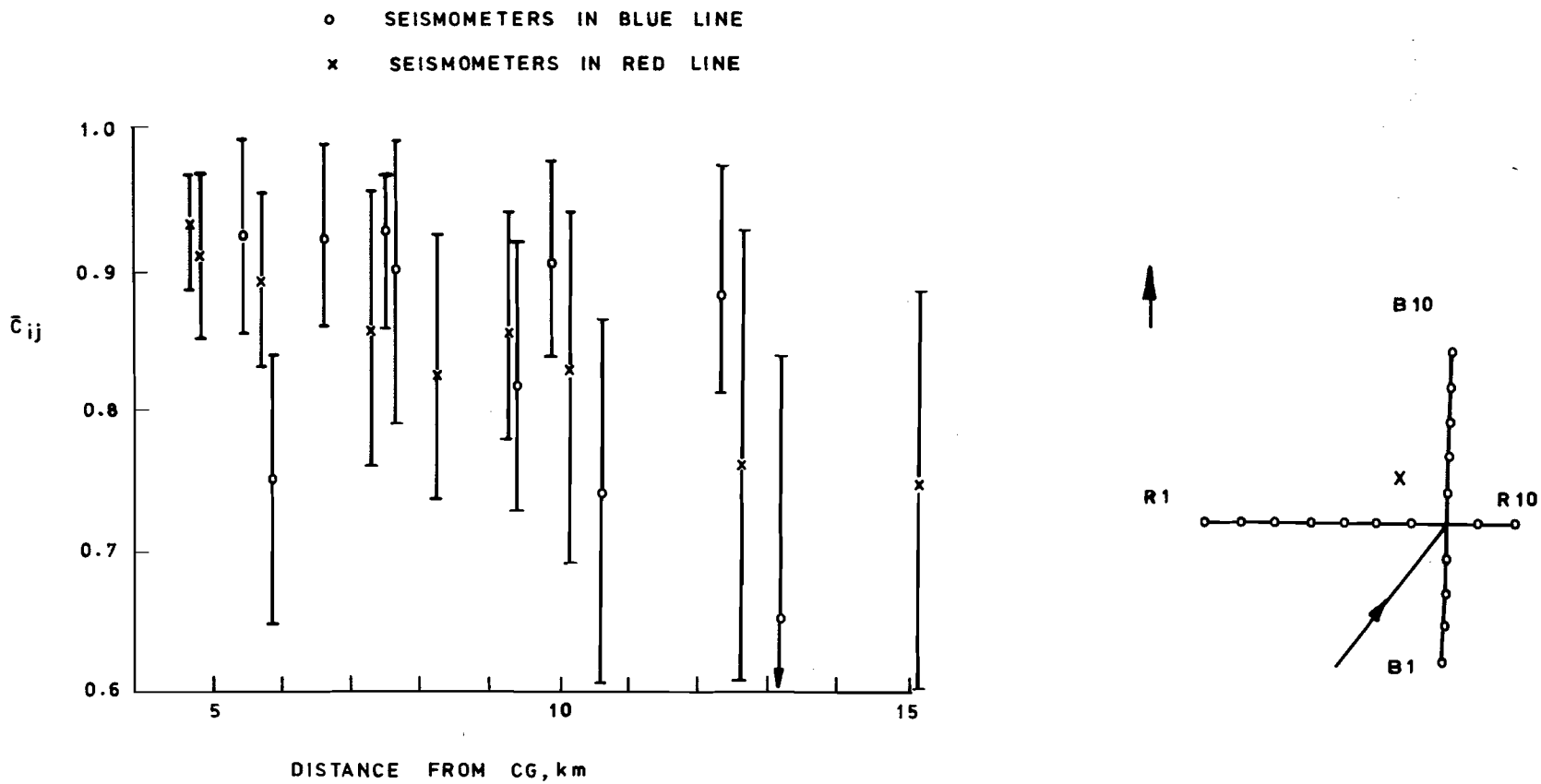

FIGURE 17. $\bar{C}_{ij}$ as a Function of Distance from the Centre of Gravity (CG) of the YKA array for the Vancouver Is earthquake of 1 January 1976. A Diagram of the array layout is given on the right of the plot and shows the Centre of Gravity (CG) of the array and an arrow indicating the Signal Azimuth.

ANNEX TO FIGURE 18

Source: Earthquake

Region: Kashmir/India/GBA

Date: 11 December 1975

Origin Time: 03-26-05.6

Latitude: 32.95N

Longitude: 76.10E

Depth: 5 km

m_b: 5.3

Known Back Bearing: N356°E

Estimated: N/A

Known Δ: 19.30°

$(R_i - P)$ Time: 5 min 40 s

Estimated Δ $(R_i - P)$: 20.0°

Tangential Error: N/A

Radial Error: 77 km

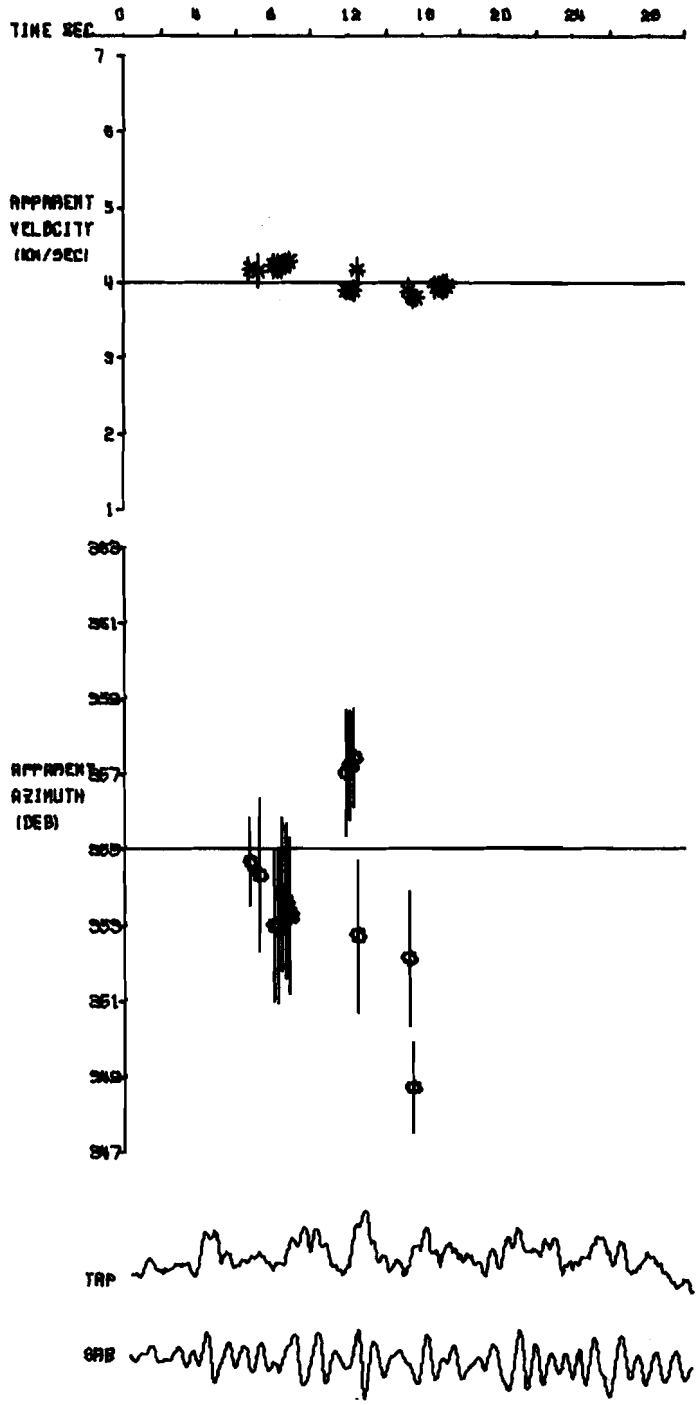
TIME SEC
0
4
8
12
16
20
24
28
APPARENT VELOCITY (KM/SEC)
7
6
5
4
3
2
1
APPARENT AZIMUTH (DEG)
363
361
359
357
355
353
351
349
347
TAP
BAB

FIGURE 18

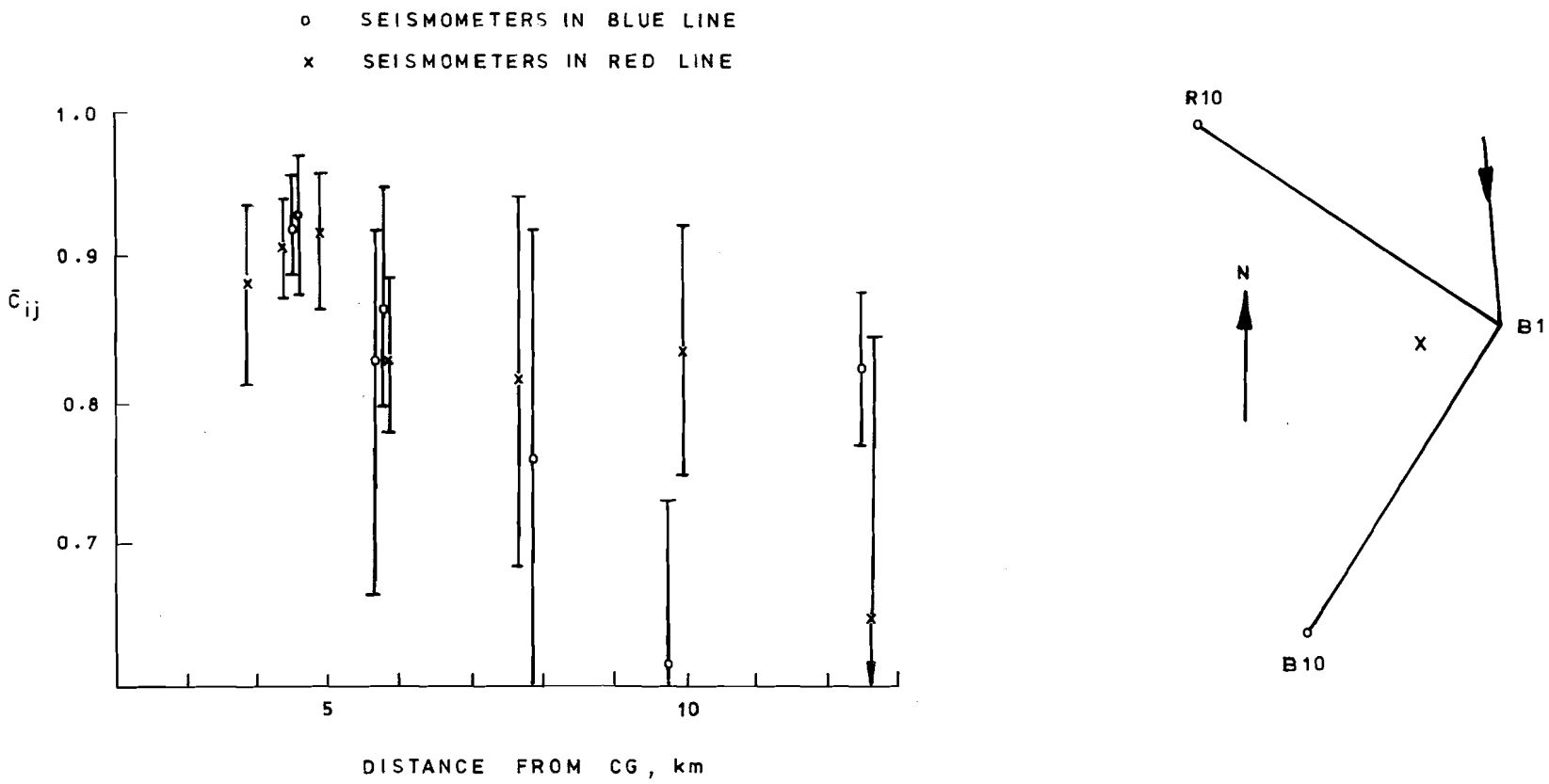

FIGURE 19. $\bar{C}_{ij}$ as a Function of Distance from the Centre of Gravity (CG) of the GBA array for the Kashmir earthquake of 11 December 1975. A Diagram of the array layout is given on the right of the plot and shows the Centre of Gravity (CG) of the array and an arrow indicating the Signal Azimuth.

ANNEX TO FIGURE 20

Source: Earthquake

Region: Tibet/India/GBA

Date: 3 October 1976

Origin Time: 15-03-43.0

Latitude: 31.91N

Longitude: 78.76E

Depth: 16.0 km

m_b: 4.7

Known Back Bearing: N003.6°E

Estimated: N003.0 ± 0.01°E

Known Δ: 18.26°

(R_i - P) Time: 5 min 20 s

Estimated Δ (R_i - P): 19.0°

Tangential Error: 21 km

Radial Error: 71 km

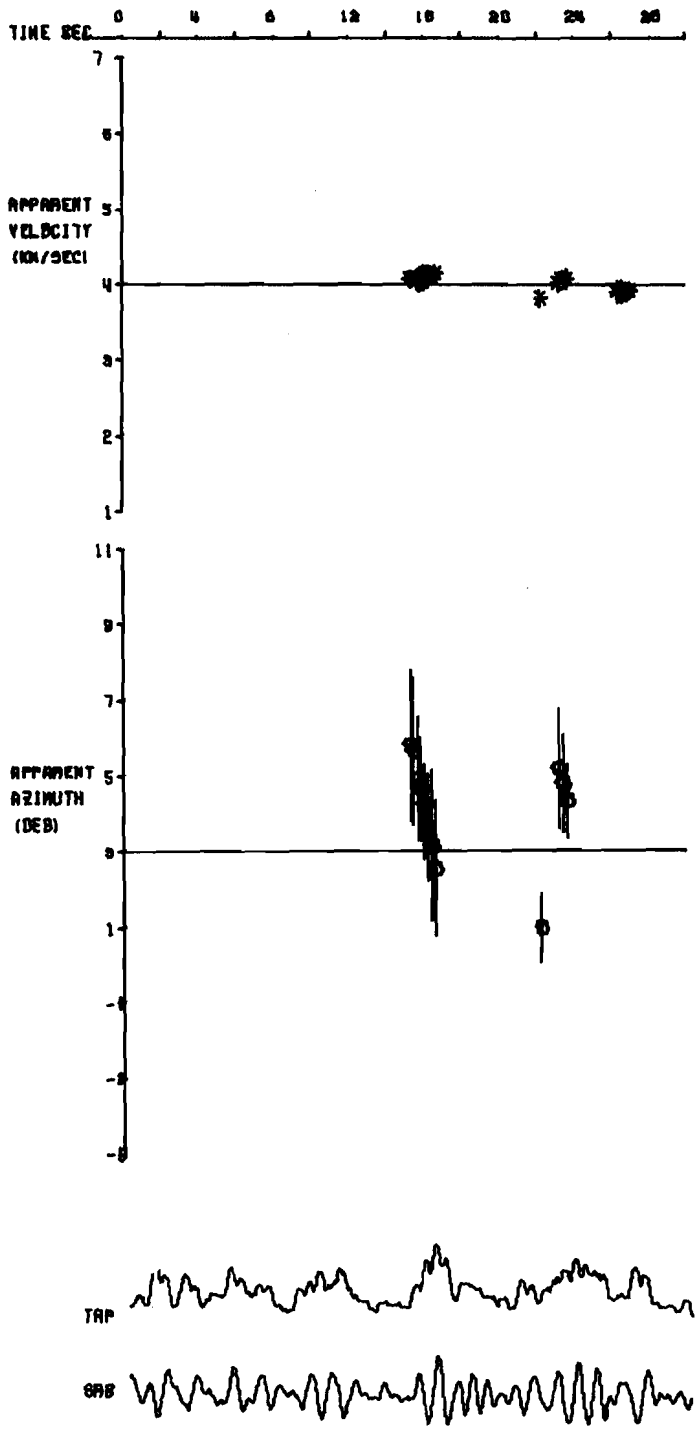
TIME SEC
0
4
8
12
16
20
24
28
APPARENT VELOCITY (KM/SEC)
7
6
5
4
3
2
1
APPARENT AZIMUTH (DEG)
11
9
7
5
3
1
-1
-3
-5
TAP
BAB

FIGURE 20

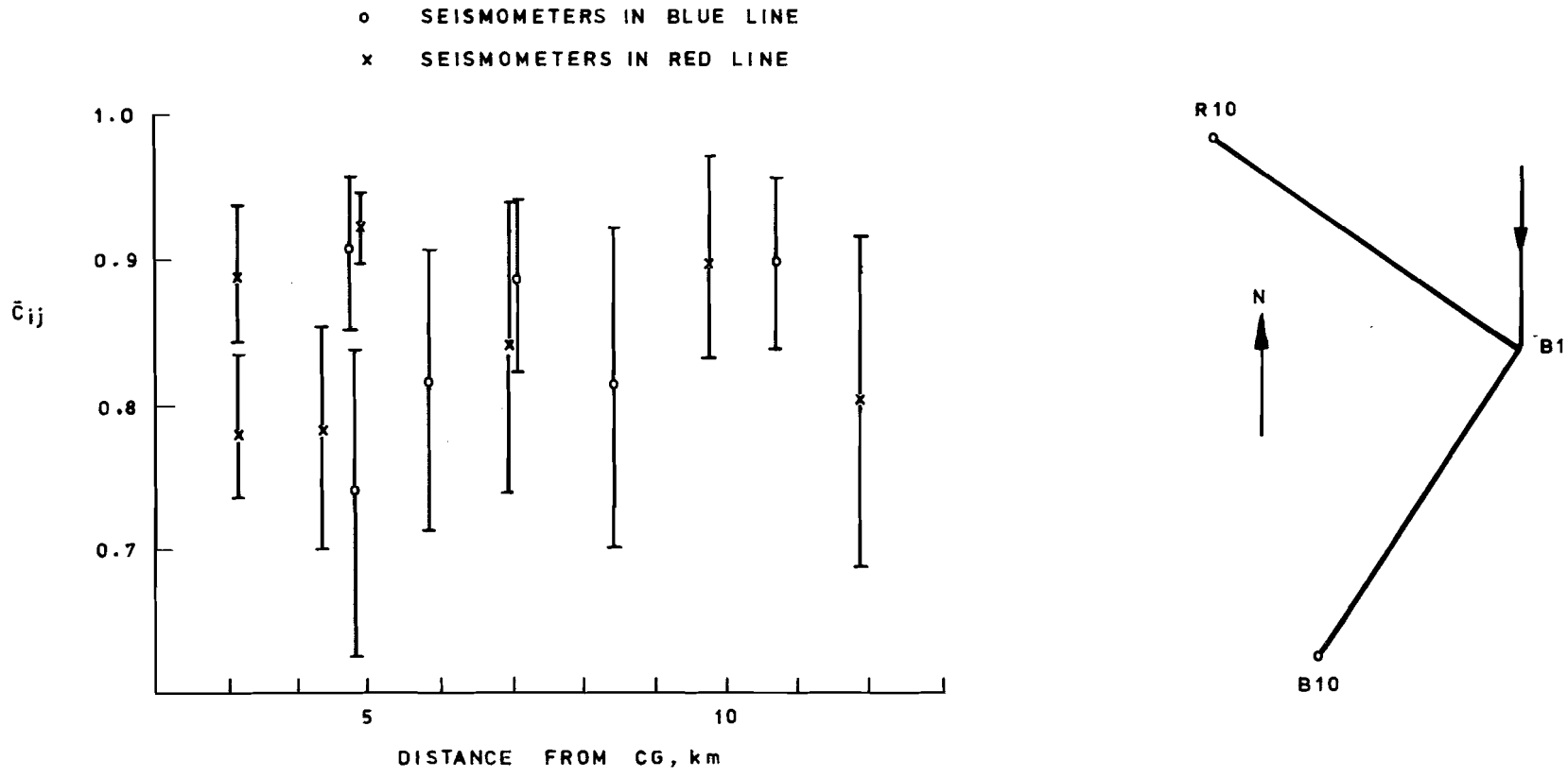

FIGURE 21. $\bar{C}_{ij}$ as a Function of Distance from the Centre of Gravity (CG) of the GBA array for the Tibetan earthquake of 3 October 1976. A Diagram of the array layout is given on the right of the plot and shows the Centre of Gravity (CG) of the array and an arrow indicating the Signal Azimuth.

APPENDIX A

THE NATURE OF R_i

We have assumed that the vertical component of the short period disturbance with typical group velocities U = 3.6 to 3.1 km/s is propagated as a higher mode Rayleigh wave. A brief summary of the evidence of this identification is given below.

Press and Ewing [2] distinguish two slow surface waves that are propagated along continental paths. They designated the waves Lg and Rg, characterised by group velocities of about 3.5 and 3.0 km/s respectively. Rg is a fundamental Rayleigh wave, quite distinct from R_i. In his intensive study of Lg and Rg, Båth [9] does not distinguish the vertical component with U $\approx$ 3.5 km/s as a different wave type from Lg, but does point out that many earthquakes which give strong, horizontal Lg motion do not produce a vertical component with similar U. (This is explicable if the excitation of R_i decreases with depth of focus more rapidly than the excitation of Lg.) Båth [9] deduced that Lg is a Love wave, with SH-type motion, but is sometimes accompanied by a small vertical component. Oliver and Ewing [10] identified this "vertical component of Lg" over Canadian paths with a particular mode of higher mode Rayleigh wave, and showed that the observed velocity dispersion is consistent with an acceptable crust and mantle velocity structure. Oliver and Ewing also display dispersion curves for higher mode Rayleigh and Love waves, travelling the same path, which show that the group velocities of both wave types tend towards U $\approx$ 3.5 km/s at short periods. This accounts for the near coincidence of the arrival times of Lg and R_i in short period seismograms. (The coincidence in group velocities occurs because short period Lg and R_i are sensitive to the SH and SV wave speeds respectively in the shallow crust. In an isotropic crust, the wave speeds of SV and SH are identical.) Panza and Calcagnile [1] show further that synthetic seismograms computed for higher mode Rayleigh waves are consistent with observed properties of R_i.

Although the above arguments about the nature of R_i are convincing, nowhere in the literature are there data on the ground motion during the passage of R_i which identifies it unequivocally as a Rayleigh wave. This appears to be because the ground motion in this group velocity window is generally confused, and difficult to interpret. If this difficulty is due to interference by S or superposition of different modes with different particle orbits, it might be possible to make sense of the ground motion at longer ranges, where S has been attenuated out and velocity dispersion has had time to separate the individual modes. The ground motion in 3.0 < U < 3.5 km/s at YKA for some NTS explosions (Δ = 25°) was, therefore, resolved into its vertical, radial and transverse components, and the vertical and radial components used to drive the X and Y sweeps of a cathode ray tube (figure A1). Since the Love wave Lg would be resolved out by this procedure, the particle orbit shown by the CRT should be elliptical, if the ground motion in the great circle plane is pure Rayleigh. In short time windows of about 5 s, this was found to be so (figures A1(a), (b) and (c)). Figure A1(d) uses the radial and transverse components (in place of vertical and radial respectively) to show that some of the transverse arrivals have no radial component, that is, they are Love waves.

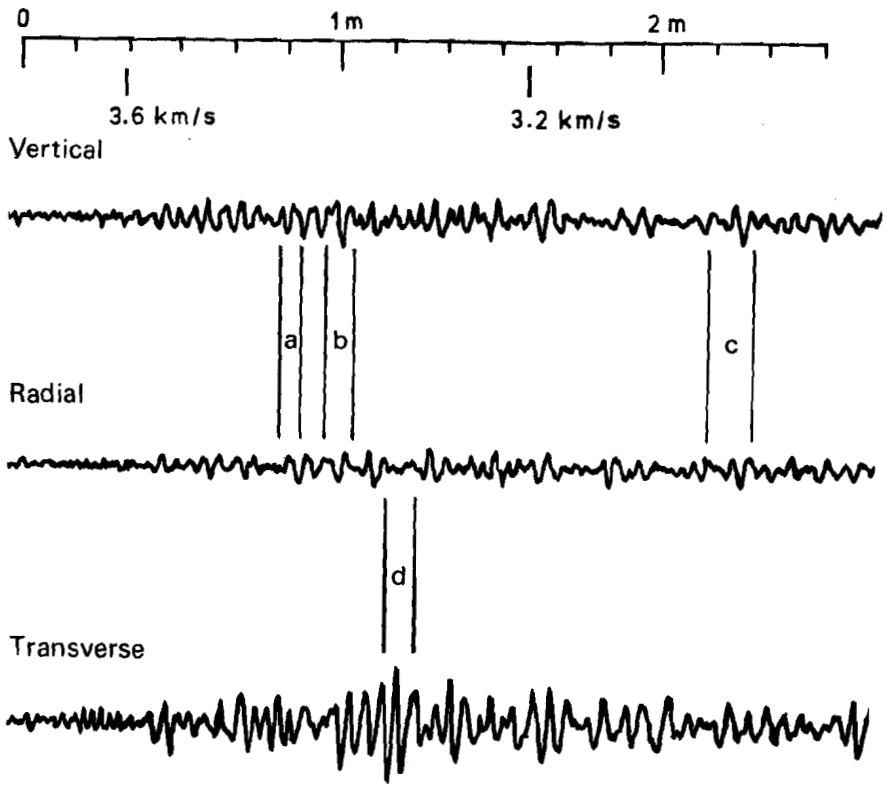

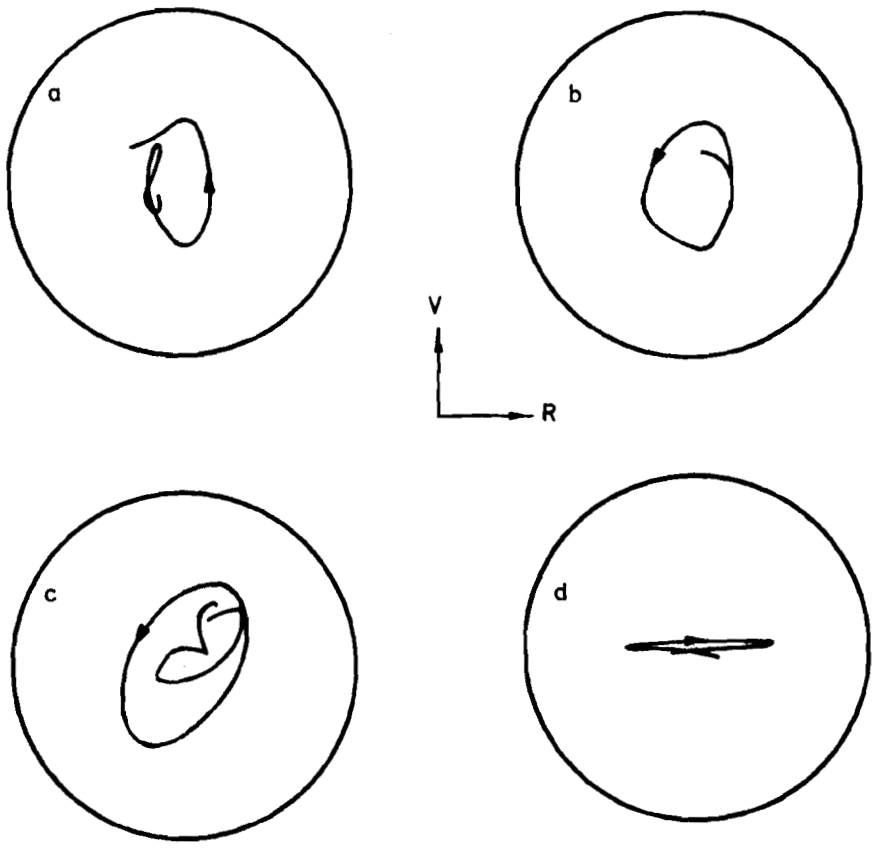

FIGURE A1. TOP: THREE COMPONENT SP SEISMOGRAMS FOR AN EXPLOSION R_1 PHASE AT YKA.

BOTTOM: CRT DISPLAYS (V = VERTICAL, R = RADIAL) OF RESOLVED PARTICLE MOTION IN TIME WINDOWS a, b, c AND d. TIME WINDOW d, DEPICTS VERTICAL AND TRANSVERSE (FOR R READ TRANSVERSE) MOTION.

APPENDIX B

THE BEST ESTIMATE OF ARRIVAL AZIMUTH

The adaptive processing of array data used in this study gives phase velocity and arrival azimuth estimates for individual regional arrivals that last 1.5 s. The estimated arrival time at each seismometer of a point of common phase in each arrival is also given. In order to make a least squares estimate of the back azimuth from receiver to source, we assume that all the R_i arrivals in a given seismogram have the same back azimuth but that phase velocities may differ. A linear equation relating phase velocity and azimuth to arrival time at each seismometer and at the centre point of the array is obtained as follows.

Consider a wavefront crossing an array (figure B1). Let the normal to the wavefront make an angle ψ with north.

Let (x_j, y_j) be Cartesian co-ordinates of the jth seismometer. Let θ_j be the angle between the north and the radius vector from the array centre point (CP) to the jth pit, a distance l_j away. Thus, if C is the arrival time at the origin of a given wavefront, the arrival time t_j at the jth seismometer is

$$t_j = C - a\ell_j \cos(\theta_j - \psi), \qquad \text{.....(B1)}$$

where $a = v^{-1}$ and v is the apparent speed. Let $\bar{a}$, $\bar{\psi}$ and $\bar{C}$ be rought estimates of a, ψ and C respectively, so

$$a = \bar{a} + \delta a; \ \psi = \bar{\psi} + \delta\psi; \text{ and } C = \bar{C} + \delta C.$$

Then (B1) becomes

$$t_j = \bar{C} + \delta C - (\bar{a} + \delta a)\ell_j \cos(\theta_j - \bar{\psi} - \delta\psi).$$

Expanding, rearranging and neglecting terms which are products of small quantities,

$$-\ell_j \cos(\theta_j - \bar{\psi})\delta a - \bar{a}\ell_j \sin(\theta_j - \bar{\psi})\delta\psi + \delta C$$

$$= t_j + \bar{a}\ell_j \cos(\theta_j - \bar{\psi}) - \bar{C}. \qquad \text{.....(B2)}$$

Consider now a series of wavefronts arriving at the array with constant azimuth ψ but different velocities v_1, v_2 .... v_n. Put $a_i = v_i^{-1}$; then, for the ith arrival, (B2) becomes

$$-\ell_j \cos(\theta_j - \psi)\delta a_i - a_i\ell_j \sin(\theta_j - \bar{\psi})\delta\psi + \delta C$$

$$= t_{ij} + a_i\ell_j \cos(\theta_j - \bar{\psi}) - \bar{C}_i.$$

For simplicity we now consider only a three seismometer array and two arrivals i = 1, 2. Equations of condition for combining the data to estimate two velocities and one azimuth are:-

$$\begin{bmatrix} 1 & 0 & -\ell_1 \cos(\theta_1 - \bar{\psi}) & 0 & -\bar{a}_1\ell_1 \sin(\theta_1 - \bar{\psi}) \\ 1 & 0 & -\ell_2 \cos(\theta_2 - \bar{\psi}) & 0 & -\bar{a}_1\ell_2 \sin(\theta_2 - \bar{\psi}) \\ 1 & 0 & -\ell_3 \cos(\theta_3 - \bar{\psi}) & 0 & -\bar{a}_1\ell_3 \sin(\theta_3 - \bar{\psi}) \\ 0 & 1 & 0 & -\ell_1 \cos(\theta_1 - \bar{\psi}) & -\bar{a}_2\ell_1 \sin(\theta_1 - \bar{\psi}) \\ 0 & 1 & 0 & -\ell_2 \cos(\theta_2 - \bar{\psi}) & -\bar{a}_2\ell_2 \sin(\theta_2 - \bar{\psi}) \\ 0 & 1 & 0 & -\ell_3 \cos(\theta_3 - \bar{\psi}) & -a_2\ell_3 \sin(\theta_3 - \bar{\psi}) \end{bmatrix} \begin{bmatrix} \delta C_1 \\ \delta C_2 \\ \delta a_1 \\ \delta a_2 \\ \delta\psi \end{bmatrix} = \begin{bmatrix} t_{11} \\ t_{12} \\ t_{13} \\ t_{21} \\ t_{22} \\ t_{23} \end{bmatrix}$$

Re-writing in matrix form $\underline{X}\,\underline{\beta} = \underline{Y}$.

The least squares estimate of β is given by the solution of

$$(\underline{X}'\underline{X})\underline{\beta} = \underline{X}'\underline{Y},$$

where X' denotes X transpose. Estimates of a_i and ψ_i are obtained as punched card output from the adaptive processing program. As a starting value for the iteration scheme described below, we put

$$\psi = \sum_{i=1}^{N} \psi_i/N$$

for the N events analysed in each R_i wavetrain. C_i and t_{ij} are also output, the latter being times relative to C_i at which peak cross-correlation occurs at the jth pit.

The following computer program (written in FORTRAN IV for an IBM370) solves

$$(\underline{X}'\underline{X})\underline{\beta} = \underline{X}'\underline{Y}$$

in a computationally efficient way, by setting up only the non-zero elements of each equation of condition, and adding the products into $\underline{X}'\underline{X}$ and $\underline{X}'\underline{Y}$ at appropriate (i,j). This procedure economises on storage by avoiding the setting up of X' and X individually and their matrix multiplication. $\underline{X}'\underline{X}$ is a (NUM*NUM) matrix, where NUM = (2* number of events) + 1, whereas X is an (ICOND*NUM) matrix, with ICOND = number of equations of condition. With the existing dimensions, the maximum allowed ICOND = 2000 (or 100 events at 20 pits), and maximum allowed NUM = 201 (or 100 events). If at the end of the second iteration,

$$\sum\sum t_{ij}^2 < \text{ICOND}*0.005s^2,$$

no further iterations are performed. A test for divergence of $\delta\psi$ with increasing number of iterations is also made. If neither condition occurs, the program stops after five iterations. The final output consists of C_j, a_i and ψ with 95% confidence limits,

$$\sum\sum t_{ij} \text{ and } \sum\sum t_{ij}^2.$$

Convergence is found to be stable and rapid and is usually complete after two iterations.

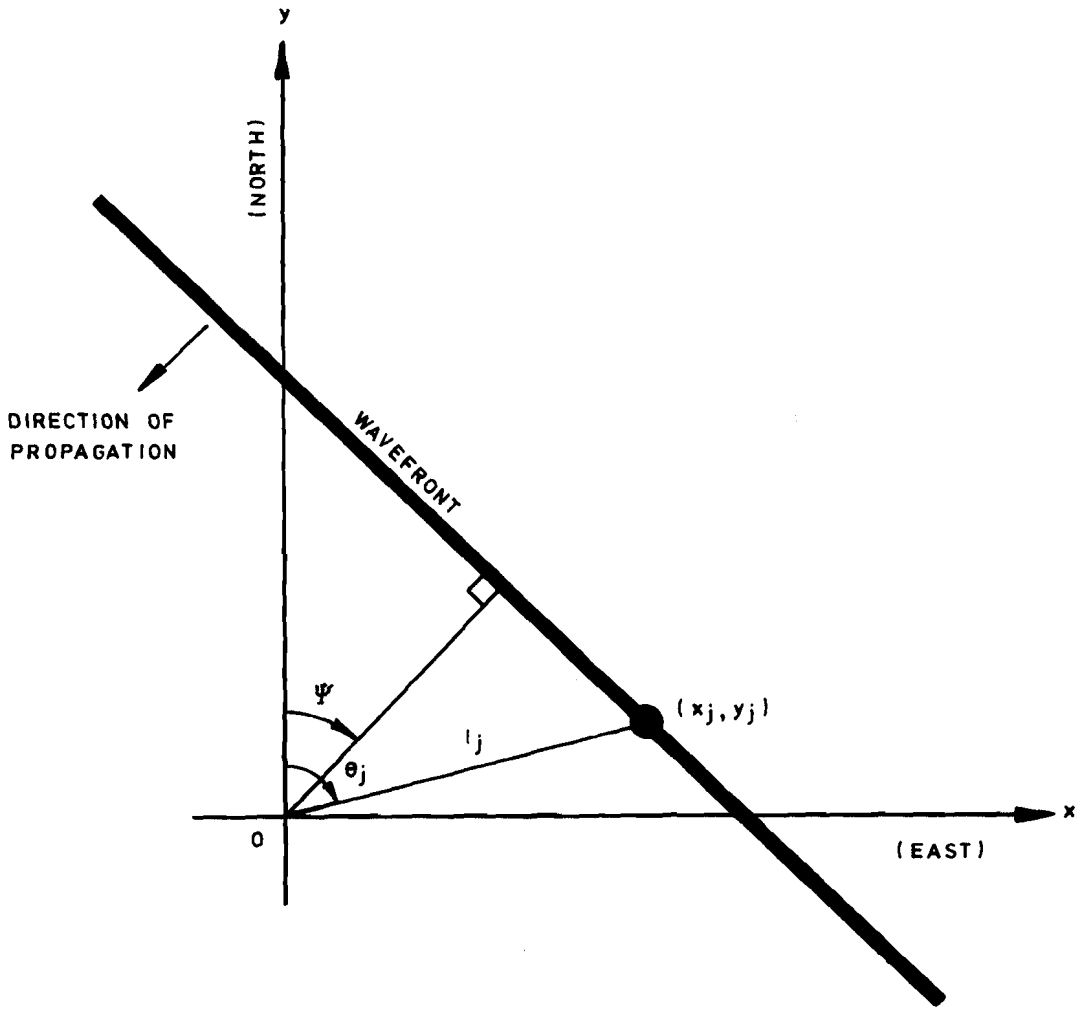

FIGURE B1. Wavefront crossing an array with Seismometers at positions (x_j, y_j) with the centre point of the array at 0

APPENDIX C

A POSSIBLE DEPTH DISCRIMINANT BASED ON THE PHASE VELOCITIES OF R_i FROM EXPLOSIONS AND EARTHQUAKES

So far, the theme of this study has been the areal location of seismic sources, using only the directional properties of R_i waves. In frequency wavenumber or (f - k) space, this is roughly equivalent to estimating angle $\gamma = \tan^{-1} k_y/k_x$ (figure C1), where k_x and k_y are mean projections of $\underline{k}$ on to the x and y axes. In estimating γ, we have not used the additional information inherent in the absolute values of $\underline{k}$, which are also determined by the adaptive processing. (In terms of phase velocity c, $|\underline{k}| = f/c$.) We now discuss the relevance of this information for depth discrimination.

Over a fixed path, the $|\underline{k}|$ population of R_i for a given source should depend on source depth, by the following reasoning. Let us consider the distribution of the horizontal component of displacement with depth for two different modes, in this case R_{II} and R_{III} (figure C2). A horizontal force at A (depth $h = h_A$) will not excite R_{III}, but will excite R_{II}, and vice versa for a source at B. This is because an antinode of R_{II} occurs at $h = h_A$, and a node at $h = h_B$; no vibration mode can be excited by a force system at a node in its pattern of displacement. In practice, how well a mode is excited depends on the variation of all components of displacement with depth and on the orientation and type of the force system. In general, however, modes with large displacements near a depth comparable with the source depth should be preferentially excited, compared to modes with nodes near the source depth.

Now the adaptive processing picks out the most energetic R_i arrivals in the instrument passband and measures their phase velocities. Since the phase velocity of a given mode is strongly influenced by the S velocity at the depth where maximum displacement occurs, the measured phase velocities should shift towards higher values for deeper travelling energy, corresponding to deeper sources.

A convincing test of this principle would require array data for R_i travelling over a fixed path for sources with known hypocentral depths. These data are not available. Those that are must be substantially affected by the path as well as the source depth. For example, most of the R_i used here have transversed extreme crustal structures such as the junction between the Rockies and Canadian Shield (YKA), or that between the Himalayas and the Deccan (GBA). It seems certain that these lateral variations change the energy partitioning between modes, as indeed might lesser features of the crust. An assessment of the importance of crustal effects must await a theoretical understanding of R_i propagation in a realistic crust. In the meantime, we present what little data we have for R_i from explosions and earthquakes.

Table C1 lists the ratio (RAT) between the number of phase velocity observations above and below 4.0 km/s obtained for each event studied. By the above reasoning, high values of RAT should crudely reflect a high proportion of deep travelling energy in the R_i wavetrain, which may be diagnostic of a deep source. (An S velocity of 4.0 km/s is typical of the base of the crust.) All of the earthquakes listed have intracrustal

depths (according to either the ISC or NEIS), but their precise depth is not known. The two explosions, on the other hand, occurred at depths less than 1.0 km. On average, therefore, the earthquake RATs should be higher than the explosion RATs. This appears to be so (table C1). Although there are undoubtedly a large number of variables other than source depth involved, this indication that RAT may be a depth (not a source) discriminant justifies further research.

TABLE C1

Ratio between the Number of R_i Phase Velocities Recorded at Greater than 4.0 km/s and Number Recorded below 4.0 km/s (Q = Earthquake, X = Explosion)

Date	Source Region	Q or X	Array	Ratio (RAT)
28 October 1975	NTS	X	YKA	1.7
7 April 1977	NTS	X	YKA	1.5
29 March 1975	Utah	Q	YKA	24.0
7 April 1975	Queen Charlotte Island	Q	YKA	3.1
9 March 1975	Akaska	Q	YKA	1.1
1 January 1976	Vancouver Island	Q	YKA	∞
11 December 1975	Kashmir	Q	GBA	1.6
3 October 1976	Tibet	Q	GBA	3.6

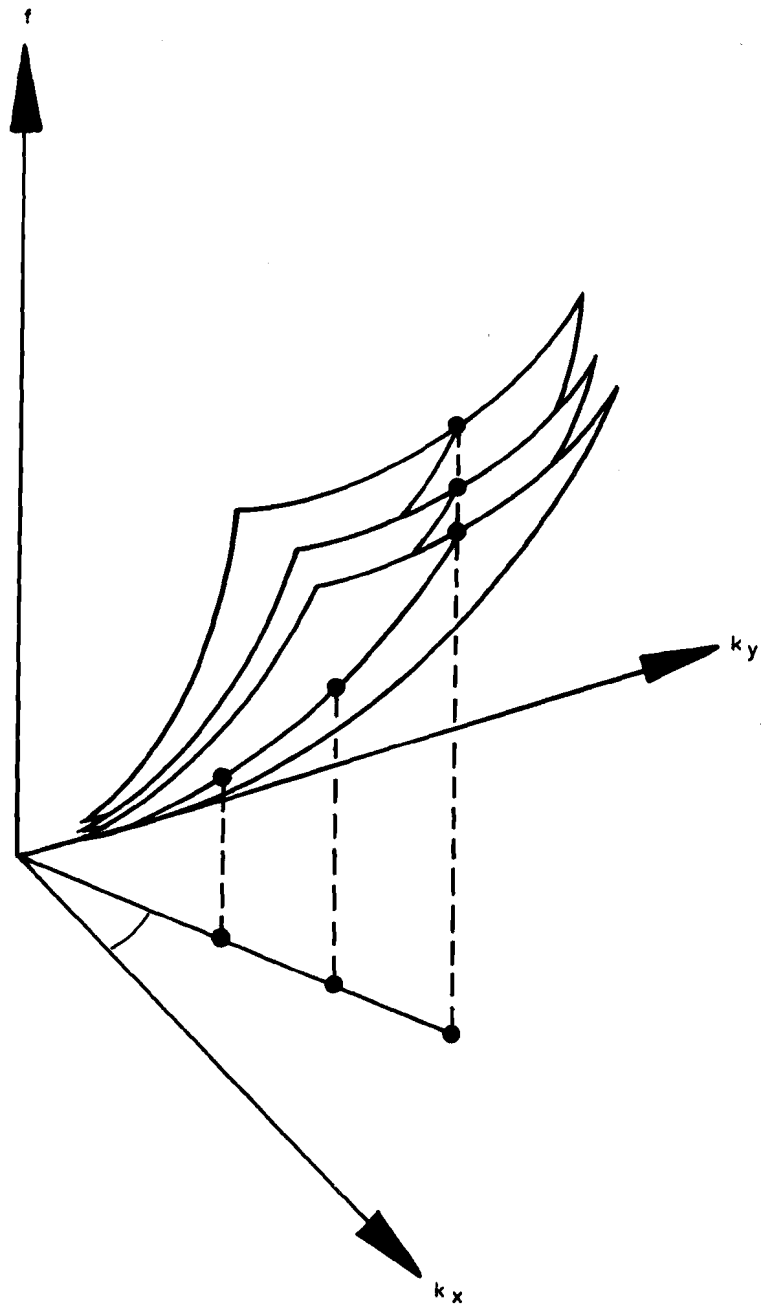

FIGURE C1. Schematic frequency-wavenumber (f-k) plot for three higher mode Rayleigh waves arriving in a range of Azimuths. The convexity of each f-k 'sheet' is due to Velocity Dispersion

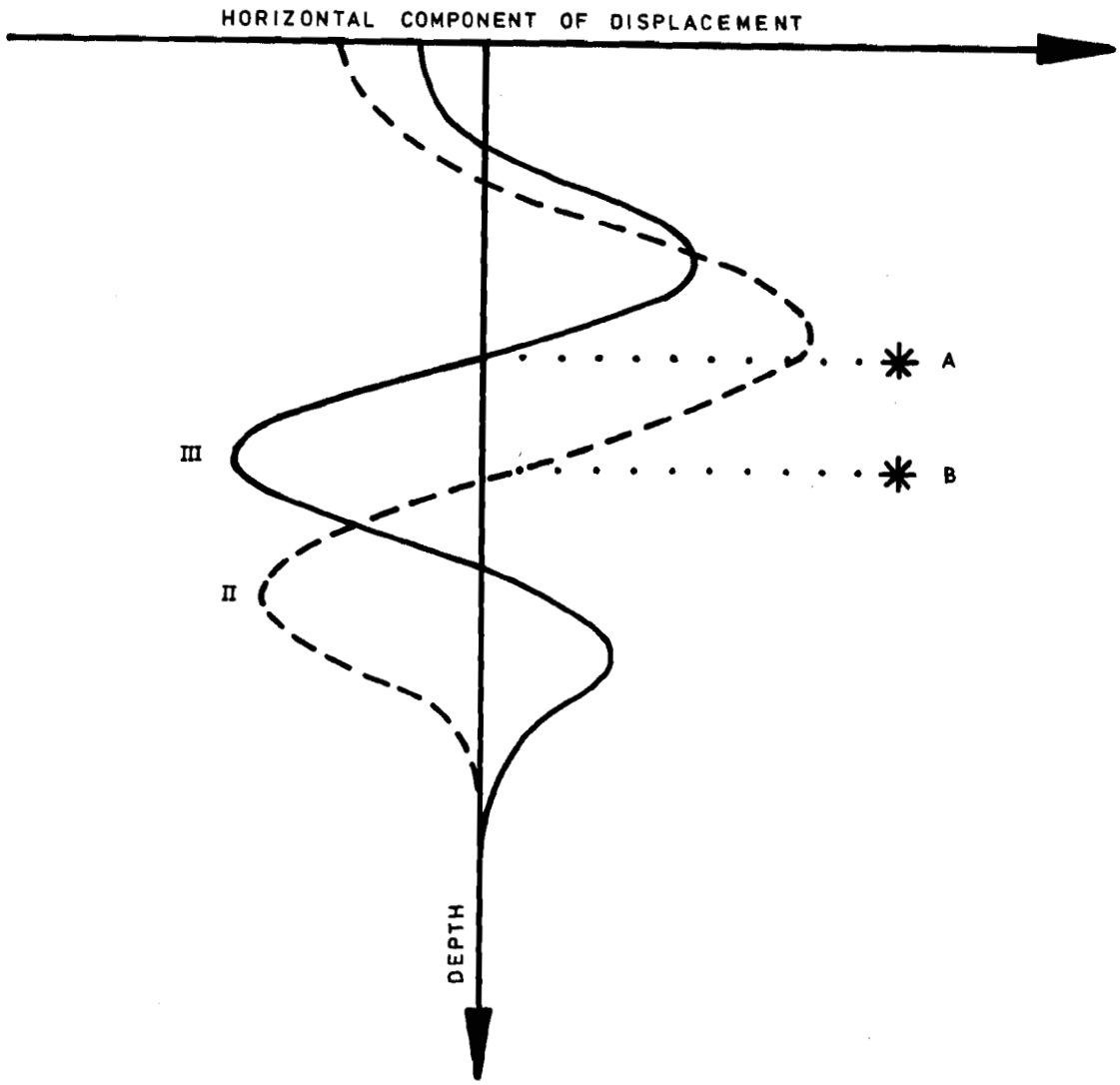

FIGURE C2 Sketch of Horizontal Displacement vs Depth plots for two Higher Modes ..... R_{II} , ——— R_{III}

DOCUMENT CONTROL SHEET

Overall security classification of sheet Unclassified

(As far as possible this sheet should contain only unclassified information. If it is necessary to enter classified information, the box concerned must be marked to indicate the classification eg (R), (C) or (S)).

1. DRIC Reference (if known)	2. Originator's Reference	3. Agency Reference	4. Report Security Classification
–	AWRE Report No. 054/78	–	Unlimited

5. Originator's Code (if known)	6. Originator (Corporate Author) Name and Location
–	Atomic Weapons Research Establishment, Aldermaston, Berkshire
5a. Sponsoring Agency's Code (if known)	**6a. Sponsoring Agency (Contract Authority) Name and Location**
–	–

7. Title On the Use of Seismometer Arrays to Locate Sources of Higher Mode Rayleigh Waves

7a. Title in Foreign Language (in the case of Translation)

–

7b. Presented at (for Conference Papers). Title, Place and Date of Conference

–

8. Author 1.Surname, Initials	9a. Author 2	9b. Authors 3, 4	10. Date	pp	ref
Barley B J	–	–	January 1979	55	10

11. Contract Number	12. Period	13. Project	14. Other References
–	–	–	–

15. Distribution Statement

No restrictions

16. Descriptors (or Keywords) (TEST)

Seismic detection
Seismic arrays
Rayleigh waves

Abstract

This report is an empirical study of higher mode Rayleigh wave (R_i) data recorded by two short period vertical seismometer arrays. Average properties of R_i such as coherence, phase velocity and relation between arrival azimuth and known back bearing are presented. The results suggest the adoption of 10 km aperture arrays with a 1 km interseismometer spacing, situated at 10° to 20° epicentral distance from the source for full exploitation of the properties of R_i.

Some Metric and SI Unit Conversion Factors

(Based on DEF STAN 00-11/2 "Metric Units for Use by the Ministry of Defence", DS Met 5501 "AWRE Metric Guide" and other British Standards)

Quantity	Unit	Symbol	Conversion
Basic Units			
Length	metre	m	1 m = 3.2808 ft 1 ft = 0.3048 m
Mass	kilogram	kg	1 kg = 2.2046 lb 1 lb = 0.45359237 kg 1 ton = 1016.05 kg
Derived Units			
Force	newton	$N = kg\ m/s^2$	1 N = 0.2248 lbf 1 lbf = 4.44822 N
Work, Energy, Quantity of Heat	joule	J = N m	1 J = 0.737562 ft lbf 1 J = 9.47817×10^{-4} Btu 1 J = 2.38846×10^{-4} kcal 1 ft lbf = 1.35582 J 1 Btu = 1055.06 J 1 kcal = 4186.8 J
Power	watt	W = J/s	1 W = 0.238846 cal/s 1 cal/s = 4.1868 W
Electric Charge	coulomb	C = A s	-
Electric Potential	volt	V = W/A = J/C	-
Electrical Capacitance	farad	F = A s/V = C/V	-
Electric Resistance	ohm	$\Omega = V/A$	-
Conductance	siemen	$S = 1\ \Omega^{-1}$	-
Magnetic Flux	weber	Wb = V s	-
Magnetic Flux Density	tesla	$T = Wb/m^2$	-
Inductance	henry	H = V s/A = Wb/A	-
Complex Derived Units			
Angular Velocity	radian per second	rad/s	1 rad/s = 0.159155 rev/s 1 rev/s = 6.28319 rad/s
Acceleration	metre per square second	m/s^2	1 m/s^2 = 3.28084 ft/s^2 1 ft/s^2 = 0.3048 m/s^2
Angular Acceleration	radian per square second	rad/s^2	-
Pressure	newton per square metre	N/m^2 = Pa	1 N/m^2 = 145.038×10^{-6} lbf/in^2 1 lbf/in^2 = 6.89476×10^3 N/m^2
	bar	bar = 10^5 N/m^2	- 1 in. Hg = 3386.39 N/m^2
Torque	newton metre	N m	1 N m = 0.737562 lbf ft 1 lbf ft = 1.35582 N m
Surface Tension	newton per metre	N/m	1 N/m = 0.0685 lbf/ft 1 lbf/ft = 14.5939 N/m
Dynamic Viscosity	newton second per square metre	$N\ s/m^2$	1 $N\ s/m^2$ = 0.0208854 $lbf\ s/ft^2$ 1 $lbf\ s/ft^2$ = 47.8803 $N\ s/m^2$
Kinematic Viscosity	square metre per second	m^2/s	1 m^2/s = 10.7639 ft^2/s 1 ft^2/s = 0.0929 m^2/s
Thermal Conductivity	watt per metre kelvin	W/m K	-
Odd Units*			
Radioactivity	becquerel	Bq	1 Bq = 2.7027×10^{-11} Ci 1 Ci = 3.700×10^{10} Bq
Absorbed Dose	gray	Gy	1 Gy = 100 rad 1 rad = 0.01 Gy
Dose Equivalent	sievert	Sv	1 Sv = 100 rem 1 rem = 0.01 Sv
Exposure	coulomb per kilogram	C/kg	1 C/kg = 3876 R 1 R = 2.58×10^{-4} C/kg
Rate of Leak (Vacuum Systems)	millibar litre per second	mb l/s	1 mb = 0.750062 torr 1 torr = 1.33322 mb

*These terms are recognised terms within the metric system.